

## Biarylpyrazole Inverse Agonists at the Cannabinoid CB1 Receptor: Importance of the C-3 Carboxamide Oxygen/Lysine3.28(192) Interaction

Dow Hurst,<sup>†</sup> Uju Umejiego,<sup>†</sup> Diane Lynch,<sup>†</sup> Herbert Seltzman,<sup>‡</sup> Steven Hyatt,<sup>‡</sup> Michael Roche,<sup>‡</sup> Sean McAllister,<sup>§</sup> Daniel Fleischer,<sup>§</sup> Ankur Kapur,<sup>§</sup> Mary Abood,<sup>§</sup> Shanping Shi,<sup>||</sup> Jannie Jones,<sup>||</sup> Deborah Lewis,<sup>||</sup> and Patricia Reggio<sup>\*†</sup>

Center for Drug Design, Chemistry and Biochemistry Department, University of North Carolina Greensboro, P.O. Box 26170, 435 New Science Building, Greensboro, North Carolina 27402-6170, Chemistry & Life Sciences, RTI International,<sup>1</sup> 3040 Cornwallis Road, Research Triangle Park, North Carolina 27709, California Pacific Medical Center Research Institute, 475 Brannan Street, Suite 220, San Francisco, California 94107, and Pharmacology and Toxicology Department, Medical College of Georgia, Augusta, Georgia 30912

Received April 14, 2006

The biarylpyrazole, *N*-(piperidin-1-yl)-5-(4-chlorophenyl)-1-(2,4-dichlorophenyl)-4-methyl-1*H*-pyrazole-3-carboxamide (SR141716; **1**) has been shown to act as an inverse agonist/antagonist at the cannabinoid CB1 receptor. Our previous mutant cycle study suggested that K3.28(192) is involved in a direct interaction with the C-3 substituent of **1** in wild-type (WT) CB1.<sup>1</sup> However, these results did not establish what part of the C-3 substituent of **1** is involved in the K3.28(192) hydrogen bond, the carboxamide oxygen or the piperidine nitrogen. Furthermore, our previous calcium channel assay results for 5-(4-chlorophenyl)-3-[(*E*)-2-cyclohexylethenyl]-1-(2,4-dichlorophenyl)-4-methyl-1*H*-pyrazole (VCHSR; **2**) (an analogue of **1** that lacks hydrogen-bonding capability in its C-3 substituent) showed that this compound acts as a neutral antagonist, a result that is in contrast to **1**, which acts as an inverse agonist in this same assay.<sup>1</sup> These results suggested a relationship between biarylpyrazole interaction with K3.28(192) at CB1 and inverse agonism, but these results were for a single pair of compounds (**1** and **2**). The work presented here was designed to test two hypotheses derived from our modeling and mutant cycle results. The hypotheses are as follows: (1) it is the carboxamide oxygen of the C-3 substituent of **1** that interacts directly with K3.28(192) and (2) the interaction with K3.28(192) is crucial for the production of inverse agonism for biarylpyrazoles such as **1**. To determine whether the carboxamide oxygen or the piperidine nitrogen of the C-3 substituent may be the interaction site for K3.28(192), we designed, synthesized, and evaluated a new set of analogues of **1** (**3–6**, Chart 1) in which modifications only to the C-3 substituent of **1** have been made. In each case, the modifications that were made preserved the geometry of this substituent in **1**. The absence of the piperidine nitrogen was not found to affect affinity, whereas the absence of the carboxamide oxygen resulted in a reduction in affinity. CB1 docking studies in an inactive state model of CB1 resulted in the trend, **3,1** < **5,4** < **2** < **6** for ligand/CB1 interaction energies. This trend was consistent with the trend in WT CB1 *K<sub>i</sub>* values versus [<sup>3</sup>H]CP55,940 reported here. In calcium channel assays, all analogues with carboxamide oxygens (**1**, **3**, and **4**) were found to be inverse agonists, whereas those that lacked this group (**2**, **5**, and **6**) were found to be neutral antagonists. Taken together, these results support the hypothesis that it is the carboxamide oxygen of the C-3 substituent of **1** that engages in a hydrogen bond with K3.28(192) in WT CB1. Furthermore, functional results for **1–6** support the hypothesis that the interaction of **1** with K3.28(192) may be key to its inverse agonism.

### Introduction

The cannabinoid CB1 receptor (Figure 1) belongs to Class A (rhodopsin (Rho) family) G-protein coupled receptors (GPCRs). CB1 receptor agonists inhibit forskolin-stimulated adenylyl cyclase by activation of a pertussis toxin-sensitive G-protein.<sup>2</sup> In heterologous cells, CB1 receptors inhibit N-, P-, and Q-type calcium channels and activate inwardly rectifying potassium channels.<sup>2–4</sup> Inhibition of calcium channels and enhancement of inwardly rectifying potassium currents is pertussis toxin-sensitive but, independent of cAMP inhibition, suggestive of a direct G-protein mechanism.<sup>3</sup>

The biarylpyrazole, *N*-(piperidin-1-yl)-5-(4-chlorophenyl)-1-(2,4-dichlorophenyl)-4-methyl-1*H*-pyrazole-3-carboxamide (SR141716; **1**) antagonizes the pharmacological and behavioral

effects produced by CB1 agonists after intraperitoneal or oral administration.<sup>5</sup> The clinical efficacy of this compound (also called rimonabant or Accomplia) for the treatment of metabolic syndrome, obesity, and smoking addiction has catalyzed massive research efforts as indicated by a surge of patent applications in recent years.<sup>6</sup> In addition to the biarylpyrazoles typified by **1**, several other heterocyclic compounds, including triazoles,<sup>7,8</sup> thiazoles,<sup>8</sup> pyrazolines,<sup>9</sup> imidazoles,<sup>8,10,11</sup> and pyridines<sup>12</sup> have been reported to be cannabinoid CB1 receptor antagonists/inverse agonists.

Compound **1** has been shown to act as a competitive antagonist and inverse agonist in host cells transfected with exogenous CB1 receptor,<sup>13</sup> in biological preparations endogenously expressing CB1<sup>14</sup> in in vitro preparations<sup>15</sup> as well as those in vivo.<sup>16</sup> Bouaboula and co-workers<sup>17</sup> reported that CHO cells transfected with human CB<sub>1</sub> receptor exhibit high constitutive activity at both levels of MAP kinase and adenylyl cyclase. Guanine nucleotides enhanced the binding of **1**, a property of inverse agonists. Lewis and co-workers<sup>13</sup> demonstrated constitutive activity of CB1 receptors in inhibiting Ca<sup>2+</sup> currents that was not due to an endogenous agonist. These investigators

\* Corresponding author. Tel: (336) 334-5333. Fax: (336) 334-5402. E-mail: phreggio@uncg.edu.

<sup>†</sup> University of North Carolina Greensboro.

<sup>‡</sup> RTI International.

<sup>§</sup> California Pacific Medical Center Research Institute.

<sup>||</sup> Medical College of Georgia.

<sup>1</sup> RTI International is a trademark of Research Triangle Institute.

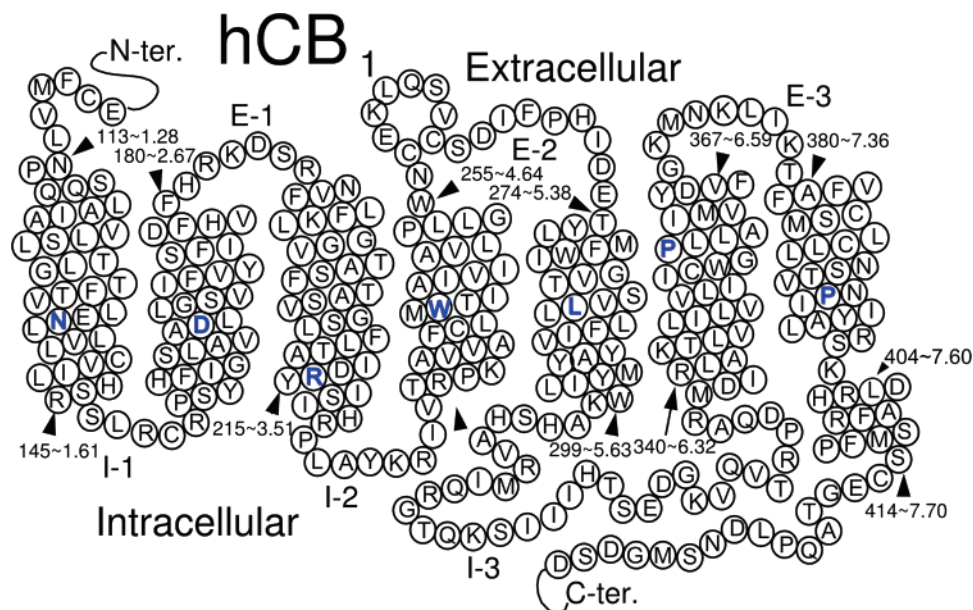


**Figure 1.** Amino acid sequence of the human CB1 receptor<sup>44</sup> is represented in helix net format here. The most highly conserved residue position in each transmembrane helix across Class A GPCRs is highlighted in blue. The Ballesteros–Weinstein amino acid numbering system<sup>42</sup> is used here (Experimental Section).

reported that **1** antagonized the Ca<sup>2+</sup> current inhibition induced by the cannabinoid agonist, (*R*)-(+)-[2,3-dihydro-5-methyl-3-[(4-morpholinyl)methyl]pyrrolo[1,2,3-*de*]-1,4-benzoxazin-6-yl]-1-naphthalenyl)methanone (WIN55212-2), in neurons heterologously expressing either rat or human CB1 receptors. Furthermore, when applied alone, **1** increased the Ca<sup>2+</sup> current with an EC<sub>50</sub> of 32 nM via a pertussis toxin-sensitive pathway, indicating that **1** can act as an inverse agonist by reversal of tonic CB1 receptor activity.

The extended ternary complex model for GPCR activation invokes the existence of two receptor conformational states, a ground or inactive R state and an active R\* state, which are in equilibrium with each other.<sup>18</sup> An agonist has higher affinity for R\*, and agonist binding is thought to shift the equilibrium toward R\*, resulting in G-protein activation with an increase in GDP/GTP exchange. An inverse agonist has higher affinity for R, and its binding shifts the equilibrium toward R, resulting in a decrease in the activation of the signaling pathway. The binding of a neutral/null antagonist is thought not to alter the equilibrium between R and R\* because the neutral antagonist has equal affinity for both states.

Our previous combined mutation/modeling studies have suggested that the binding site of the CB1 inverse agonist/antagonist, **1**, is within the transmembrane helix (TMH)3-4-5-6 aromatic microdomain and involves direct aromatic stacking interactions with F3.36(200), Y5.39(275), and W5.43(279).<sup>19</sup> Our modeling studies have also suggested that although **1** can engage in aromatic stacking interactions in the inactive (R) and active (R\*) states of CB1, the C-3 substituent carboxamide oxygen of **1** can hydrogen bond with K3.28(192) only in the CB1 inactive (R) state (Figure 2).<sup>1</sup> We hypothesized that this interaction may be responsible for the higher affinity of **1** for the inactive state, rendering it an inverse agonist. (For a discussion of the creation of the activated (R\*) state model and experimental evidence supporting its creation, please see Experimental Section.) To test this hypothesis, a mutant thermodynamic cycle was constructed that combined the evaluation of the affinity of **1** at wild-type (WT) CB1 and the CB1 K3.28(192)A mutant with an evaluation of the WT CB1 and K3.28(192)A affinities of an analogue of **1**, 5-(4-chlorophenyl)-

3-[(*E*)-2-cyclohexylethenyl]-1-(2,4-dichlorophenyl)-4-methyl-1*H*-pyrazole (**2**), which lacks hydrogen-bonding potential in its C-3 substituent but maintains aromatic stacking interactions analogous to **1** in R and R\*.<sup>1</sup> Mutant cycle results suggested that K3.28(192) is involved in a direct interaction with the C-3 substituent of **1** in WT CB1 and that K3.28(192) does not interact with **2**. However, these results did not establish what part of the C-3 substituent of **1** is involved in the K3.28(192) hydrogen bond because there are two potential hydrogen bond acceptors in this substituent, the carboxamide oxygen and the piperidine nitrogen. Furthermore, calcium channel assay results for **2** at WT CB1 showed that this compound acts as a neutral antagonist, a result that is in contrast to **1**, which acts as an inverse agonist in this same assay.<sup>1</sup> These results supported our hypothesis that there may be a relationship between biarylpyrazole interaction with K3.28(192) at CB1 and inverse agonism, but these results were for a single pair of compounds (**1** and **2**).

The work presented here was designed to test two hypotheses: (1) it is the carboxamide oxygen of the C-3 substituent of **1** that interacts directly with K3.28(192) and (2) the interaction with K3.28(192) is crucial for the production of inverse agonism for biarylpyrazoles such as **1**. To determine whether the carboxamide oxygen or the piperidine nitrogen of the C-3 substituent may be the hydrogen bond acceptor for K3.28(192), we designed, synthesized and evaluated a new set of analogues of **1** (**3–6**, Chart 1) in which modifications to the C-3 substituent have been made. Results reported here support the hypothesis that it is the carboxamide oxygen of the C-3 substituent of **1** that engages in a hydrogen bond with K3.28(192) in WT CB1. Furthermore, functional results for **3–6** support the hypothesis that the interaction of **1** with K3.28(192) may be key to its inverse agonism because all analogues that retained carboxamide oxygens were found to act as inverse agonists, while even high CB1 affinity analogues that lacked the carboxamide oxygen such as 5-(4-chlorophenyl)-1-(2,4-dichlorophenyl)-4-methyl-3-[(*E*)-piperidinoinimomethyl]-1*H*-pyrazole (**5**) were found to act as neutral antagonists.

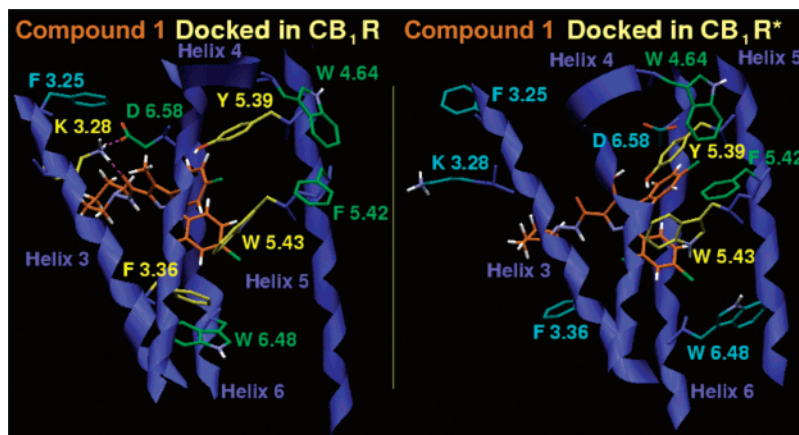
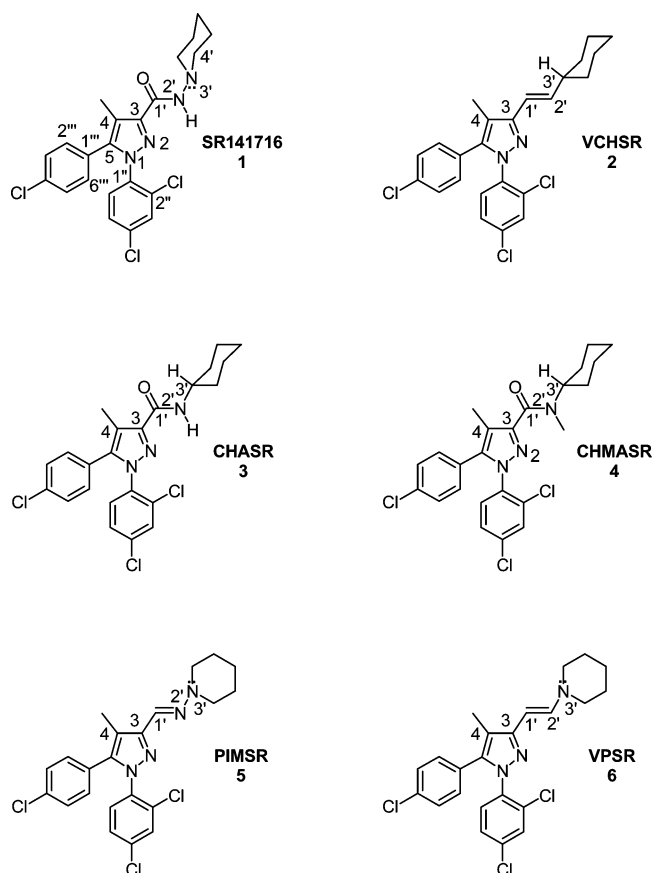


**Figure 2.** Compound **1** in a minimum energy conformation ( $\Delta E = 0.92$  kcal/mol) docked in the computer TMH bundle model of the R state of CB1. The view here is from the lipid, looking toward TMH4. Residues with which **1** has direct interactions are colored yellow. Residues that form part of the aromatic cluster complex with **1** but that do not stack directly with **1** are colored green. Residues that have no direct or indirect interaction with **1** are colored cyan. (Left) The R state model is characterized by a salt bridge between K3.28(192) and D6.58(366) and two patches of aromatic residues that form clusters in the TMH3-4-5-6 region of CB1, W5.43(279)/F3.36(200)/W6.48(356), and Y5.39(275)/W4.64(255)/F5.42(278). (Right) In the R\* state, the K3.28(192)-D6.58(366) salt bridge is broken due to rotations of TMHs 3 and 6 and a conformational change in TMH6. The aromatic cluster in this region has rearranged with F5.42(278)/W4.64(255)/Y5.39(275)/W5.43(279), forming a cluster. It is clear here that although **1** has aromatic stacking interactions that allow it to be part of the TMH3-4-5-6 aromatic microdomain in both R and R\*, **1** is able to engage in hydrogen bonding (with K3.28(192)) only in the R state.

### Chart 1



### Results

**Conformational Analysis.** Figure 3 illustrates the global minimum energy conformers of compounds **3**, **4**, and **2**. Figure 4 illustrates the global minimum energy conformers of compounds **1**, **5**, and **6** in yellow, superimposed at their pyrazole rings with the initial docked conformation of each shown in pink.

**Compound 1 Global Minimum Energy Conformer.** The global minimum energy conformer of **1** (Figure 4, left, yellow)

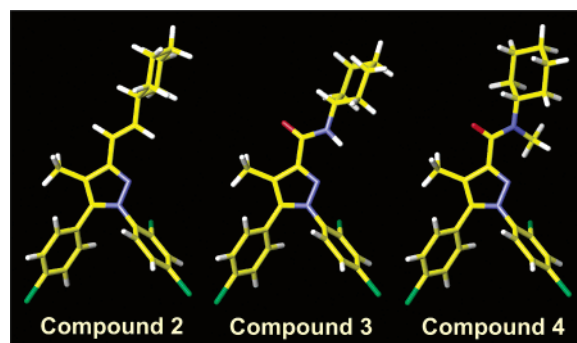


**Figure 3.** Global minimum energy conformers of compounds **3**, **4**, and **2** as initially identified by the AM1 semiempirical method and then optimized by ab initio Hartree–Fock 6-31G\* calculations.

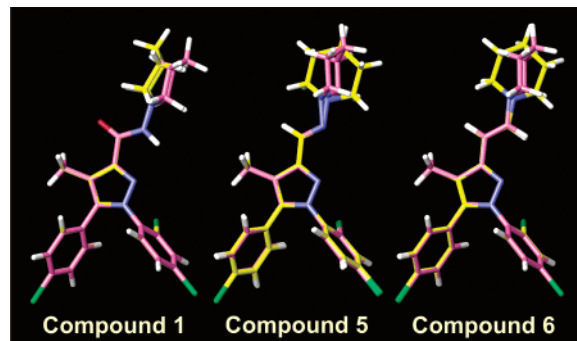


**Figure 4.** Global minimum energy conformers of compounds **1**, **5**, and **6** (in yellow) as initially identified by the AM1 semiempirical method and then optimized by ab initio Hartree–Fock 6-31G\* calculations. Illustrated in pink is the higher minimum energy conformation for **1**, **5**, and **6** used for initial docking studies. The energies of these conformers were obtained from ab initio Hartree–Fock 6-31G\* calculations as described in the Experimental Section. The calculated energy expenses for each ligand to assume its initially docked conformation were the following: **1**,  $\Delta E = 0.92$  kcal/mol; **5**,  $\Delta E = 0.51$  kcal/mol; and **6**,  $\Delta E = 4.55$  kcal/mol.

has the carboxamide oxygen of the C3 substituent nearly in plane with the pyrazole ring and pointing in the direction of the C4 methyl group ( $O-C1'-C3-C4 = 0.7^\circ$ ). (See Chart 1 for the numbering system.) The piperidine ring is in a chair

conformation with the nitrogen lone pair of electrons pointing in the same direction as the carboxamide hydrogen (LP-N3'-N2'-H = 0.2°). The monochlorophenyl ring is out of plane with the pyrazole ring (C4-C5-C1'''-C2''' = -59.7°), and the dichlorophenyl ring is also out of plane with the pyrazole ring (N2-N1-C1''-C2'' = -75.6°). In this position, the *ortho*-chloro is in the bottom face of the molecule (i.e., below the plane of the page). In the global minimum energy conformer of **1** shown in Figure 4, the carboxamide group is in a *trans* geometry. This carboxamide group *trans* geometry was found to be lower in energy than a *cis* geometry by 4.81 kcal/mol at the HF 6-31G\* level. We also found in docking studies that the *cis* form had severe steric clashes with TMH7; therefore, only the *trans* geometry was considered further. A recent crystal structure of **1** confirms the carboxamide group *trans* geometry (George, C. Laboratory for the Structure of Matter, Naval Research Laboratory. Personal communication).

**Compound 2 Global Minimum Energy Conformer.** The global minimum energy conformer of **2** (Figure 3, right) differs from that of **1** only in the orientation of its cyclohexyl ring compared with that of the piperidine ring in **1**. In the global minimum of **2**, the *trans*-ethylene group is oriented such that the hydrogen attached to C1' is nearly in the plane of the pyrazole ring, pointing toward the C4 methyl group (H-C1'-C3-C4 = -2.6°), and the hydrogen attached to C3' (cyclohexyl ring) points in the opposite direction from the C2' hydrogen (H-C3'-C2'-H = 177.5°).

**Compound 3 Global Minimum Energy Conformer.** The global minimum energy conformer of **3** (Figure 3, left) is analogous to that of **2** and differs from that of **1** only in the orientation of its cyclohexyl ring compared with that of the piperidine ring in **1**. In the global minimum of **3**, the carboxamide group is oriented such that the carboxamide oxygen is nearly in the plane of the pyrazole ring, pointing toward the C4 methyl group (O-C1'-C3-C4 = -2.5°), and the hydrogen attached to C3' (cyclohexyl ring) points in the opposite direction from the amide hydrogen (H-C3'-N2'-H = -158.7°).

**Compound 4 Global Minimum Energy Conformer.** The global minimum energy conformer of **4** (Figure 3, middle) differs from that of **1** in the orientation of its cyclohexyl ring compared with that of the piperidine ring in **1**. In the global minimum of **4**, the *N*-methyl amido group is oriented such that the carboxamide oxygen is closer to C4 methyl group than to the pyrazole N2. Unlike **2** and **3**, the amido group is not in the plane of the pyrazole ring, but is rotated out of plane due to a steric clash between the *N* methyl and the pyrazole N2 nitrogen (O-C1'-C3-C4 = 26.3°). The hydrogen attached to C3' (cyclohexyl ring) points in the opposite direction from the amido *N* methyl (H-C3'-N2'-C = -168.4°).

**Compounds 5 and 6 Global Minimum Energy Conformers.** Figure 4 illustrates the global minimum energy conformers of **5** (center) and **6** (right). The global minimum energy conformers of **5** and **6** differ from that of **1** in that their piperidine rings are rotated nearly 90° about the 2'-3' bond relative to that of **1**. Such an orientation presumably allows the piperidine nitrogen lone pair of electrons to resonate with the C=N or C=C pi systems, respectively (LP-N3'-N2'-C1' = 99.1°; LP-N3'-C2'-C1' = 104.8°). The *trans*-C=N or *trans*-ethylene group is oriented such that the hydrogen attached to C1' is nearly in the plane of the pyrazole ring, pointing toward the C4 methyl group (H-C1'-C3-C4 = -2.8° and 7.3°, respectively).

**Conformer Selection for Docking.** In our initial study of **1**,<sup>1</sup> we chose not to dock **1** in its global minimum energy conformation (Figure 4, left, yellow) in our model of the CB1

inactive state but rather in another minimum energy conformation (Figure 4, left, pink). A molecular electrostatic potential (MEP) map calculated at the AM1 level (data not shown) indicated that the piperidine nitrogen of **1** generates an MEP minimum (i.e., negative potential region) second only to that generated by the carboxamide oxygen in **1**. AM1 conformational searches identified another minimum energy conformation of **1** in which the piperidine nitrogen's lone pair points in the direction opposite to that of the carboxamide hydrogen (LP-N3'-N2'-H = 178.8°). An MEP of this conformer showed an enhanced negative potential region associated with the C-3 substituent. Although AM1 calculations showed that this conformer was 4.83 kcal/mol higher in energy than the global minimum, ab initio Hartree-Fock 6-31G\* calculations indicated that the energy separation between these two conformers was only 0.92 kcal/mol. For docking studies, we chose to use this minimum energy conformer of **1** (Figure 4, left, pink), a conformation that is mimicked by the global minimum energy conformations of **3**, **4**, and **2** (Figure 3). The conformations used for docking **5** and **6** were analogous to the docked conformation of **1** (Figure 4, middle and right, pink). Hartree-Fock 6-31G\* calculations ab initio indicated that the energy separation between these initially docked conformers and their respective global minimum energy conformers (Figure 4, middle and right, yellow) were 0.51 kcal/mol for **5** and 4.55 kcal/mol for **6**.

**Receptor Docking.** There are two features of the CB1 R TMH bundle model that appear to be important for the binding of biarylpyrazoles such as **1** at CB1. The first is a salt bridge formed by K3.28(192) and D6.58(366). The second is the aromatic residue-rich TMH3-4-5-6 region of the CB1 model, which is characterized by a W6.48(356)/W5.43(279)/F3.36(200) and a Y5.39(275)/W4.64(255)/F5.42(278) aromatic cluster in the CB1 R state. We begin here by separately discussing these two features of the CB1 R TMH bundle model.

**K3.28(192) and D6.58(366) Salt Bridge.** One of the significant features of our CB1 R TMH bundle model is a salt bridge between K3.28(192) and D6.58(366) (N-O distance = 2.6 Å; N-H-O angle = 159°). Unlike the intracellular R3.50/E6.30 (or R3.50/D6.30) salt bridge suggested to stabilize G-protein-coupled receptors (GPCRs) in their inactive states,<sup>20,21</sup> the extracellular K3.28(192)/D6.58(366) salt bridge (present only in the inactive state of CB1) seems to be important for positioning K3.28(192) for ligand interaction in the inactive state rather than for stabilizing the receptor in the inactive state. In fact, Pan and co-workers<sup>13</sup> found that WT CB1 and the CB1 K3.28(192)A mutant exhibit the same level of constitutive activity. Therefore, the absence of the K3.28(192)/D6.58(366) salt bridge does not lead to greater ease of activation. The K3.28(192)/D6.58(366) salt bridge is made possible by two special structural features of the CB1 receptor, its extracellular loop 2 (EC-2) loop and the flexibility of TMH6 in CB1. Despite the fact that the CB1 and CB2 receptors belong to the Class A (rhodopsin (Rho)) family of GPCRs, there are important differences between CB1/CB2 and Rho that impact the ligand binding pocket in the TMH3-4-5-6 region. The CB1 and CB2 EC-2 loops are shorter than that of Rho (CB1, 15 residues in length; CB2, 13 residues in length; Rho, 25 residues in length), and there is no corresponding Cys residue in TMH3 of CB1 or CB2 that would cause the EC-2 loop to dip down into the binding site crevice as the EC-2 disulfide bridge with Cys3.25-(110) causes in Rho. However, in CB1 there is an EC-2 Cys residue near the extracellular end of TMH4 (C257) and a Cys near the middle of the EC-2 loop (C264) that have been shown to be essential for high-level expression and CB1 receptor

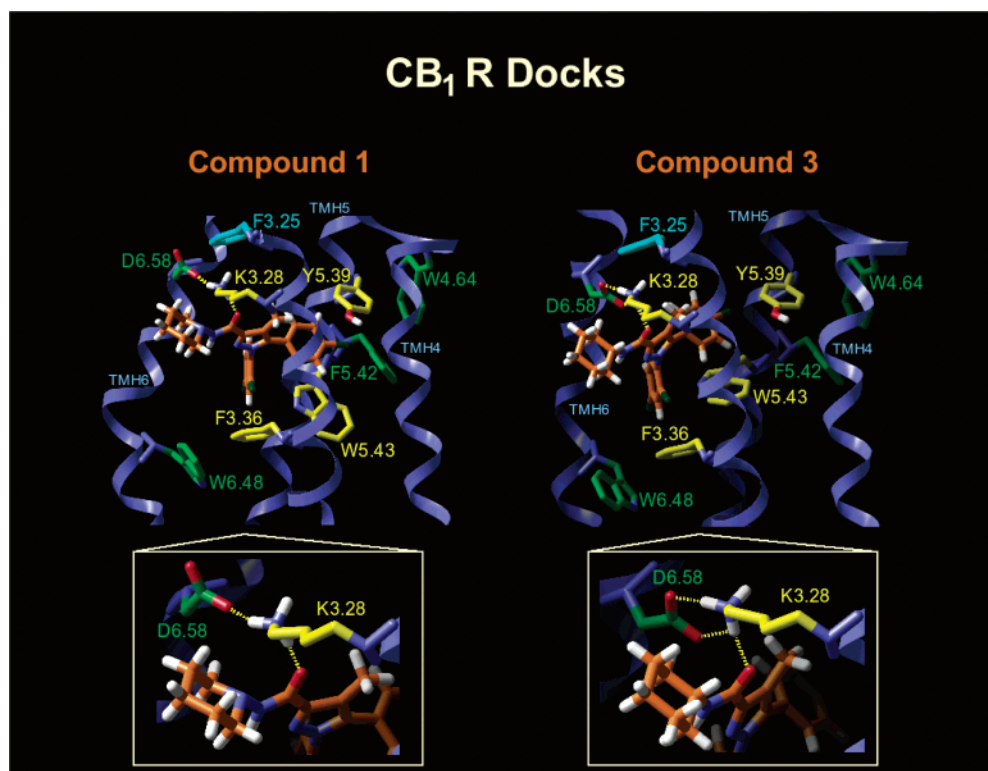


**Figure 5.** (Left) Compound **1** and (Right) compound **3** in their energy minimized complexes with the model of the inactive (R) state of CB1. The conformational energy expense for each ligand relative to its global minimum in its final energy minimized complex was 1.26 kcal/mol for **1** and 0.00 kcal/mol for **3**. The view here is from the lipid, looking between TMHs 5 and 6. The R state is characterized by a salt bridge between K3.28(192) and D6.58(366) and two patches of aromatic residues that form clusters in the TMH3-4-5-6 region of CB1, W5.43(279)/F3.36(200)/W6.48(356), and Y5.39(275)/W4.64(255)/F5.42(278). Residues with which ligands have direct interactions are colored here in yellow. Residues that form part of the aromatic cluster complex with ligand, but do not stack directly with the ligand are colored green. Residues that have no direct or indirect interaction with the ligand are colored cyan. (Left) The carboxamide oxygen of **1** has a hydrogen-bonding interaction with K3.28(192) in the salt bridge (inset). Because **1** directly stacks with F3.36(200), Y5.39(275), and W5.43(279), the ligand joins the F3.36(200)/W5.43(279)/W6.48(356) and Y5.39(275)/W4.64(255)/F5.42(278) aromatic clusters into one large extended cluster in the minimized complex. (Right) The carboxamide oxygen of **3** has a hydrogen-bonding interaction with K3.28(192) in the salt bridge (inset) and **3** has aromatic stacking interactions with F3.36(200), Y5.39(275), and W5.43(279). In binding, CHASR (**3**) bridges between the F3.36(200)/W5.43(279)/W6.48(356) and Y5.39(275)/W4.64(255)/F5.42(278) aromatic clusters and helps form one large extended cluster in the minimized complex.

function.<sup>22</sup> This result combined with mutation results for the corresponding pair of Cys residues in CB2 (C174 and C179)<sup>23</sup> suggests that a disulfide bridge between these two Cys residues may exist. As the result of this important difference between Rho and the CB receptors, the binding site crevice around TMHs 3-4-5-6 is likely to be different, with the EC-2 loop occupying less volume in the upper part of the binding pocket than the EC-2 loop in Rho. The different spatial requirements of the EC-2 loop are important because this difference permits the extracellular end of TMH6 to occupy a different position in the TMH bundle than that seen in Rho. We have shown that the small size of residue 6.49 in CB1 (a Gly) results in the pronounced flexibility of the CWXP motif in TMH6.<sup>24</sup> This motif has been suggested to function as a flexible hinge, permitting agonist-promoted movement of the intracellular end of TMH6 that occurs during activation.<sup>25,26</sup> In addition to permitting the intracellular end of TMH6 to come close to the intracellular end of TMH3 in the inactive state of CB1, this flexibility in CB1 TMH6 permits the extracellular end of TMH6 to bend toward TMH3, resulting in the formation of a salt bridge between D6.58(366) (near the extracellular end of TMH6) and K3.28(192) in TMH3. In the active state (R\*) TMH bundle model, the K3.28(192) and D6.58(366) salt bridge is broken (N-O distance = 16.8 Å). The change in the positions of K3.28(192) and D6.58(366) from the R to R\* state in our CB1 models can be seen in Figure 2. As will be discussed below, we found

that compounds **1-6** fell into two different categories based upon their hydrogen bonding capabilities with K3.28(192).

**TMH3-4-5-6 Aromatic Microdomain.** Both the CB1 inverse agonist/antagonist **1** and compounds **2-6** are highly aromatic compounds. We hypothesized that aromatic stacking interactions might be important for the binding of these compounds at CB1. The CB1 TMH3-4-5-6 region is rich in aromatic residues that face into the ligand binding pocket, including F3.25(189), F3.36(200), W4.64(255), Y5.39(275), W5.43(279), and W6.48(356). Shire and co-workers<sup>23</sup> have shown in CB1/CB2 chimera studies that the TMH4-EC2-TMH5 region of CB1 contains residues critical for the binding of **1**. In Monte Carlo/stochastic dynamics simulations of the inactive state of WT CB1,<sup>27</sup> we found a persistent aromatic stack between Y5.39(275) and W4.64(255) that seemed to be important for stabilizing the positions of TMHs 4 and 5 in the TMH bundle on the extracellular side and a second aromatic stack between F3.36(200), W5.43(279), and W6.48(356) that seemed to be open for additional interaction with the ligand. Subsequent CB1 F3.36(200)A, W5.43(279)A, and W6.48(356)A mutation studies indicated that the binding of **1** is affected by each of these mutations, suggesting that these residues are part of the binding site for **1**.<sup>19</sup> Therefore, compounds **1-6** were docked in the aromatic residue-rich TMH3-4-5-6 region of the CB1 model here. Our inactive state (R) bundle model in the TMH3-4-5-6 region is characterized by a W6.48(356)/W5.43(279)/F3.36(200) and a

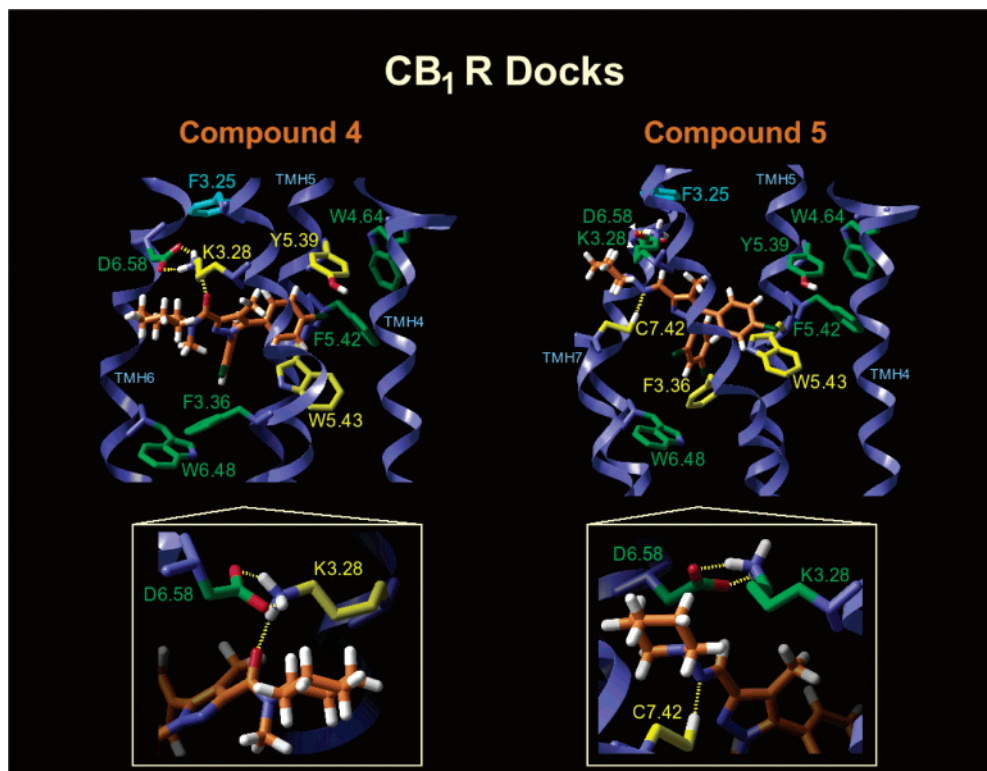


**Figure 6.** (Left) Compound **4** and (Right) compound **5** in their energy minimized complexes with the model of the inactive (R) state of CB1. The conformational energy expense for each ligand relative to its global minimum in its final energy minimized complex was 0.12 kcal/mol for **4** and 1.29 kcal/mol for **5**. The view here is from the lipid, looking between TMHs 5 and 6. For a description of the R state, please see Figure 5 caption. Residues with which ligands have direct, indirect, or no interaction are colored here in yellow, green, or cyan, respectively. (Left) The carboxamide oxygen of **4** has a hydrogen-bonding interaction with K3.28(192) in the salt bridge (inset). Because **4** directly stacks with both Y5.39(275) and W5.43(279), the ligand joins the F3.36(200)/W5.43(279)/W6.48(356) and Y5.39(275)/W4.64(255)/F5.42(278) aromatic clusters into one large extended cluster in the minimized complex. (Right) Compound **5** has no interaction with K3.28(192) in the salt bridge (inset). The piperidine nitrogen of **5**, however, forms a hydrogen bond with C7.42(386). Compound **5** also has direct aromatic stacking interactions with F3.36(200) and W5.43(279). Although **5** does not stack directly with Y5.39(275), Y5.39(275) has a direct offset parallel stacking interaction with W5.43(279) ( $d = 6.9 \text{ \AA}$ ). Therefore, **5** is part of the larger TMHs 3-4-5-6 aromatic cluster in the minimized complex.

Y5.39(275)/W4.64(255)/F5.42(278) aromatic cluster. We found that each ligand could insert itself into this aromatic residue-rich region to become an integral part of an extended aromatic cluster.

**Ligand/CB1 R Complexes.** The energy minimized ligand/CB1 inactive (R) state complexes for compounds **1**–**6** are illustrated in Figures 5–7. Aromatic residues for which each ligand has a direct aromatic stacking interaction are colored yellow in Figures 5–7. Aromatic residues that are part of the extended aromatic cluster are colored green and those that are not part of the binding pocket are colored cyan. Aromatic stacking interactions are summarized in Table 1 according to the measured distance between ring centroids ( $d$ ) and the angle ( $\alpha$ ) between normal vectors of interacting aromatic rings for each ligand/CB1 R minimized complex.

Table 2 presents the energy decomposition for each ligand/CB1 R complex. This Table includes all residues that line the ligand binding pocket of each ligand and their pairwise interaction energy with each ligand. The interaction energy includes both Coulombic and van der Waals components. We found that for all ligands, van der Waals interactions with V3.32(196), T3.33(197), and M6.55(363) contributed significantly to the overall pairwise interaction energies. Other significant interactions are discussed below for each individual ligand. In addition to calculating the pairwise interaction energies, we also analyzed the output from our minimized ligand/CB1 R complexes and assessed if the ligand remained in its initial docked conformation or adjusted its conformation in the presence of

the receptor. HF-6-31G\* single point calculations were performed on the conformation of each ligand in the final energy minimized ligand/receptor complex in order to determine the energy difference between the global minimum energy conformer and the final ligand conformation in the minimized ligand/CB1 R complex. These differences are summarized in Table 2 (second to last row) and are discussed for each individual ligand below as well.

Figure 5 illustrates the energy minimized complexes, compound **1**/CB1 R (left) and compound **3**/CB1 R (right). The conformation of **1** in this minimized complex is 1.26 kcal/mol above the global minimum for **1** (Table 2), whereas **3** remains in its global minimum in the energy minimized complex. The R state is characterized by a salt bridge between K3.28(192) and D6.58(366) and two patches of aromatic residues that form clusters in the TMH3-4-5-6 region of CB1, W5.43(279)/F3.36(200)/W6.48(356), and Y5.39(275)/W4.64(255)/F5.42(278). The carboxamide oxygen of **1** has a hydrogen-bonding interaction with K3.28(192) in the salt bridge (inset). The hydrogen bond (N–O) distance and (N–H–O) angles for this interaction are 2.65 Å, 156°, respectively. This result is consistent with our previous K3.28(192)A mutation results that suggest a direct interaction between **1** and K3.28(192).<sup>1</sup> Because **1** directly stacks with both F3.36(200) and W5.43(279) and with Y5.39(275) (Table 1), the ligand bridges the F3.36(200)/W5.43(279)/W6.48(356) and Y5.39(275)/W4.64(255)/F5.42(278) aromatic clusters present in the TMH3-4-5-6 aromatic microdomain to form an extended aromatic cluster in the minimized complex.

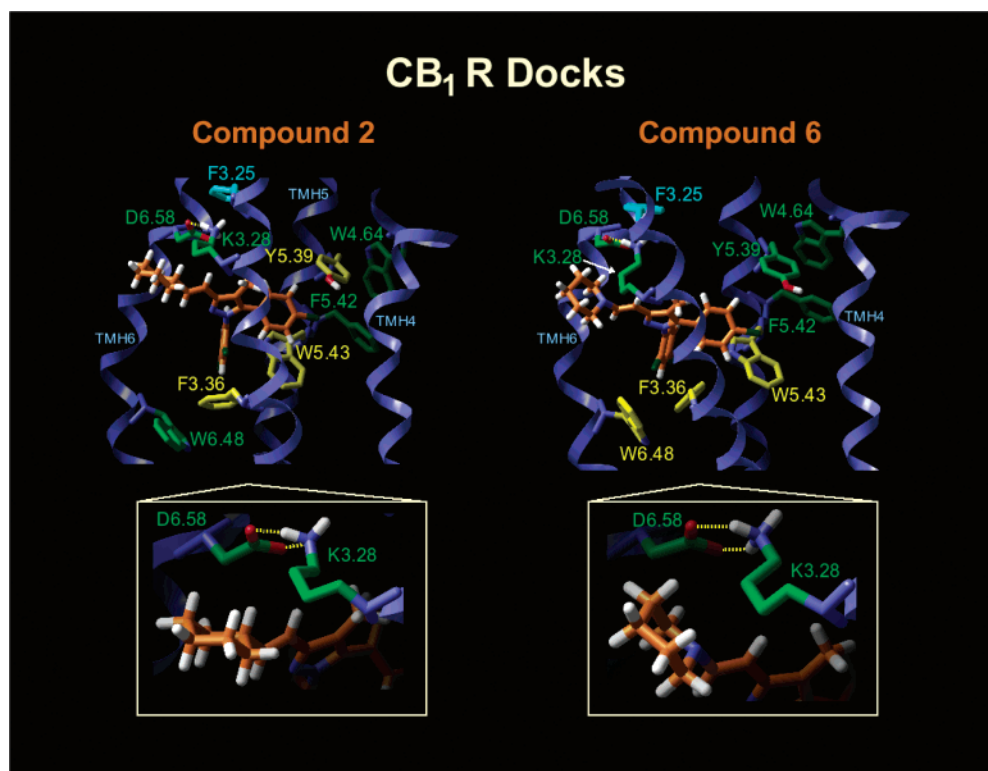


**Figure 7.** (Left) Compound **2** and (Right) compound **6** in their energy minimized complexes with the model of the inactive (R) state of CB1. The conformational energy expense for each ligand relative to its global minimum in its final energy minimized complex was 0.16 kcal/mol for **2** and 4.57 kcal/mol for **6**. The view here is from the lipid, looking between TMHs 5 and 6. For a description of the R state, please see Figure 5 caption. Residues with which ligands have direct, indirect, or no interaction are colored here yellow, green, or cyan, respectively. Neither **2** nor **6** is capable of interacting with the K3.28(192) and D6.58(366) salt bridge (see insets). However, both ligands can interact with the TMH3-4-5-6 aromatic cluster. (Left) Compound **2** directly stacks with F3.36(200), Y5.39(275), and W5.43(279). This permits the ligand to be part of the TMH3-4-5-6 extended aromatic cluster in the minimized complex. (Right) Compound **6** directly stacks with F3.36(200), W5.43(279), and W6.48(356). Although **6** does not stack directly with Y5.39(275), Y5.39(275) has a direct offset parallel stacking interaction with W5.43(279) ( $d = 6.7$  Å). Therefore, **6** is part of the larger TMH3-4-5-6 aromatic cluster in the minimized complex.

**Table 1.** Aromatic Stacking Interactions Identified for Compounds 1–6 in the CB1 R Model

compd	F3.36		Y5.39		W5.43 Ring A <sup>e</sup>		W5.43 Ring B <sup>f</sup>		W6.48– Ring A	
	$d^c$ (Å)	$\alpha^d$ (deg)	$d$ (Å)	$\alpha$ (deg)	$d$ (Å)	$\alpha$ (deg)	$d$ (Å)	$\alpha$ (deg)	$d$ (Å)	$\alpha$ (deg)
<b>SR 1</b>										
MC ring <sup>a</sup>	6.9	56	6.0	60	4.7	44	5.8	44		
DC ring <sup>b</sup>	5.3	65			5.2	86				
<b>VCHSR 2</b>										
MC ring			5.9	41	3.5	OP <sup>g</sup>	4.7	OP		
DC ring	5.4	76			4.2	77	5.3	77		
<b>CHASR 3</b>										
MC ring			5.9	35	3.7	OP	4.5	OP		
DC ring	4.6	52			4.9	75	5.3	75		
<b>CHMASR 4</b>										
MC ring			5.0	49	4.6	20	6.0	20		
DC ring					4.9	89				
<b>PIMSR 5</b>										
MC ring	6.5	30			4.0	25	5.1	25		
DC ring	4.4	40			5.5	75				
<b>VPSR 6</b>										
MC ring	6.2	33			4.9	45	5.9	45		
DC ring	4.3	34			5.8	70			6.8	51

<sup>a</sup> MC = monochlorophenyl ring. <sup>b</sup> DC = dichlorophenyl ring. <sup>c</sup>  $d$  = distance between aromatic ring centroids. <sup>d</sup>  $\alpha$  = angle between normal vectors of interacting rings. <sup>e</sup> Ring A = five-membered ring. <sup>f</sup> Ring B = six-membered ring. <sup>g</sup> OP = offset parallel stack.

In Figure 5 (right), the carboxamide oxygen of **3** has a hydrogen-bonding interaction with K3.28(192) in the salt bridge (inset). The hydrogen bond (N–O) distance and (N–H–O) angle

for this interaction are 2.67 Å and 154°, respectively. Compound **3** also has direct aromatic stacking interactions with F3.36(200) and W5.43(279) and with Y5.39(275) (Table 1). In binding, **3** also bridges between the F3.36(200)/W5.43(279)/W6.48(356) and Y5.39(275)/W4.64(255)/F5.42(278) aromatic clusters and helps form one large extended cluster in the minimized complex.

Figure 6 illustrates the energy minimized complexes, compound **4**/CB1 R (left) and compound **5**/CB1 R (right). The conformation of **4** in this minimized complex is 0.12 kcal/mol above its global minimum (Table 2), whereas the conformation of **5** is 1.29 kcal/mol above its global minimum. Despite the fact that the global minimum of **4** has its carboxamide group rotated out of the plane of the pyrazole ring, **4** is still able to engage in a hydrogen-bonding interaction between its carboxamide oxygen and K3.28(192) as can be seen in Figure 6 (left; inset). Compound **4** directly stacks with both W5.43(279) and with Y5.39(275) but lacks an aromatic stacking interaction with F3.36(200) (Table 1). This is due to the steric interference caused by its N methyl. Because **4** directly stacks with both W5.43(279) and with Y5.39(275), however, it joins the F3.36(200)/W5.43(279)/W6.48(356) and Y5.39(275)/W4.64(255)/F5.42(278) aromatic clusters into one large extended cluster in the minimized complex.

In Figure 6 (right), compound **5** has no interaction with K3.28(192) in the salt bridge (inset). The imino nitrogen of **5** (N2' in Chart 1), however, forms a hydrogen bond with C7.42(386). The hydrogen bond (N–S) distance and (N–H–S)

**Table 2.** Pairwise Interaction Energies for Compounds 1–6 with CB1 R Binding Pocket Residues, Conformational Energy Expense for Each Ligand Dock, and the Combined Energy for Each Ligand/CB1 R Complex

Coulomb kJ/mol	SR141716	VCHSR	CHASR	CHMASR	PIMSR	VPSR
K3.28	-72.02	6.54	-54.64	-65.99	6.25	3.44
L3.29	0.53	0.02	0.65	-0.21	0.32	0.49
V3.32	-1.04	0.34	-1.05	0.05	-3.26	-3.15
T3.33	-1.29	0.27	-1.72	-1.02	-1.80	-2.12
F3.36	-1.11	-2.05	-3.93	-0.60	-1.53	-1.25
T3.37	0.02	0.66	0.66	1.04	-1.11	-0.05
I4.56	-0.74	0.26	0.32	0.31	-0.39	-0.60
Y5.39	-1.02	1.27	-0.32	1.60	0.15	0.81
W5.43	-0.70	-0.39	1.26	-0.64	3.44	2.53
W6.48	-0.31	-0.20	0.35	0.04	-0.53	0.69
I6.54	0.25	-0.75	-0.01	0.26	-2.84	-0.92
M6.55	2.49	-0.35	1.89	1.14	-5.56	-7.00
D6.58	5.67	-9.80	3.36	9.50	-9.28	-8.30
F7.35	-0.12	-0.63	-0.44	-0.33	-1.68	-1.48
C7.38	-0.24	0.34	-0.08	-0.47	0.44	-0.34
S7.39	-0.85	-0.03	-0.50	-0.38	-0.67	-0.85
C7.42	1.71	-0.45	1.07	1.38	-8.56	9.05
subtotal (kJ/mol)	-68.77	-4.97	-53.14	-54.31	-26.61	-9.04
subtotal (kcal/mol)	-16.43	-1.19	-12.69	-12.97	-6.35	-2.16
vdW kJ/mol	SR141716	VCHSR	CHASR	CHMASR	PIMSR	VPSR
K3.28	-8.81	-8.05	-5.64	-3.96	-8.59	-13.85
L3.29	-9.99	-5.02	-6.62	-9.20	-5.69	-7.02
V3.32	-20.29	-15.51	-16.86	-19.60	-19.23	-22.57
T3.33	-11.01	-9.40	-14.31	-11.18	-15.61	-17.26
F3.36	-14.39	-11.96	-15.52	-5.82	-23.50	-24.99
T3.37	-2.86	-2.18	-2.53	-3.00	-2.68	-3.76
I4.56	-3.61	-6.37	-5.73	-4.60	-1.82	-2.03
Y5.39	-6.59	-10.01	-8.79	-15.04	-4.12	-3.50
W5.43	-25.10	-42.01	-36.20	-28.69	-31.46	-20.02
W6.48	-0.84	-1.25	-5.26	-1.52	-2.83	-9.16
I6.54	-3.13	-4.77	-0.99	-0.48	-5.47	-6.09
M6.55	-28.36	-30.14	-31.40	-21.83	-26.48	-20.08
D6.58	-6.75	-10.23	-12.35	-7.18	-8.62	-4.14
F7.35	-1.03	-9.17	-1.67	-0.45	-8.02	-4.55
C7.38	-0.61	-4.59	-1.18	-1.18	-3.13	-4.62
S7.39	-5.75	-5.79	-3.22	-6.17	-4.65	-5.77
C7.42	-6.03	-6.04	-4.24	-5.10	-10.25	-5.16
subtotal (kJ/mol)	-155.14	-182.48	-172.51	-145.01	-182.15	-174.55
subtotal (kcal/mol)	-37.05	-43.59	-41.20	-34.63	-43.51	-41.69
total (kJ/mol)	-223.91	-187.45	-225.66	-199.31	-208.76	-183.60
total (kcal/mol)	-53.48	-44.77	-53.90	-47.61	-49.86	-43.85
ligand conf. cost <sup>a</sup> (kcal/mol)	1.26	0.16	0.00	0.12	1.29	4.57
combined total (kcal/mol)	-52.22	-44.61	-53.90	-47.48	-48.57	-39.29

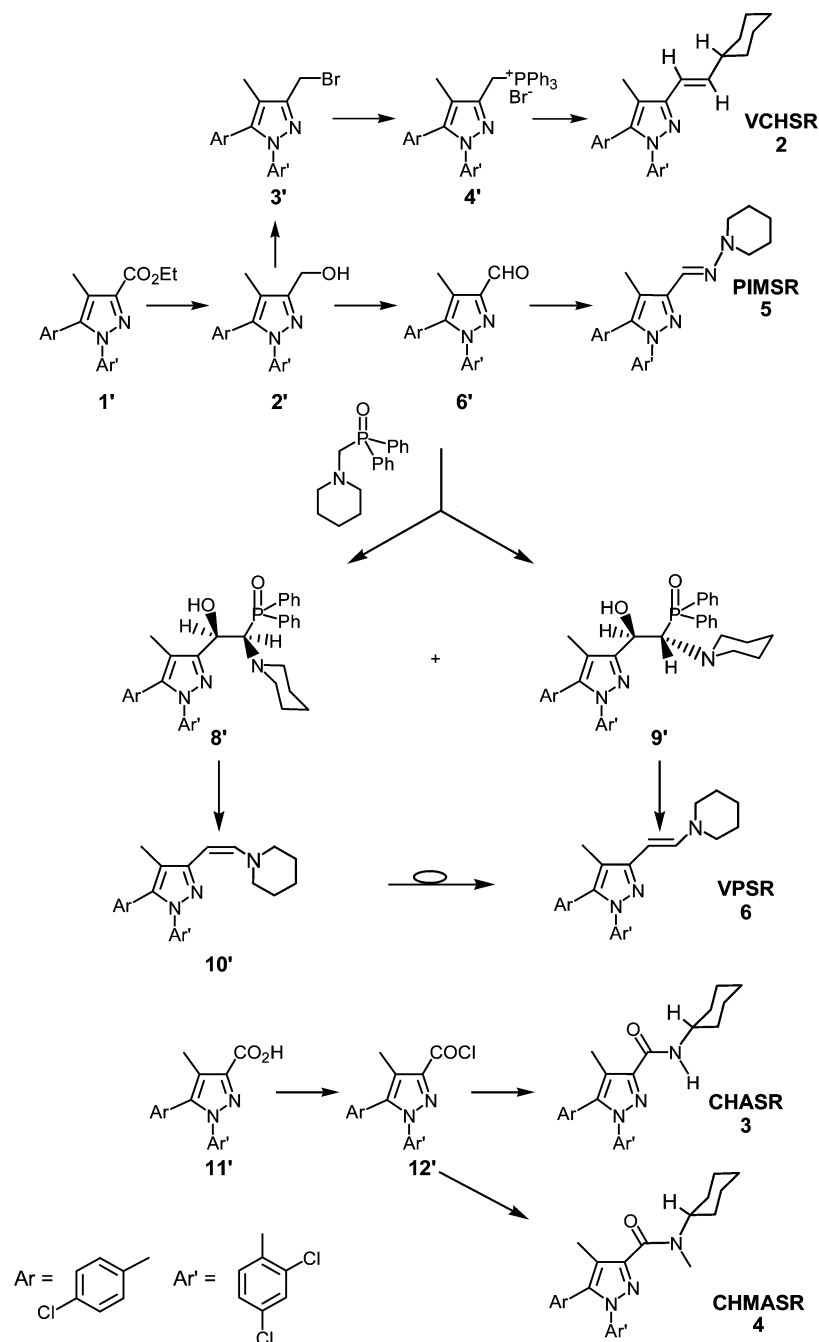
<sup>a</sup> Energy calculated at the HF-6-31G\* level (see Experimental Section).

angle for the interaction with C7.42(386) are 3.32 Å, 174°, respectively, for **5**. In recent CB1 cysteine reactivity studies, Fay and co-workers found that C7.42(386) is reactive toward methanethiosulfonate (MTS) sulfhydryl labeling agents and is, thus, solvent accessible. Steric bulk introduced at this site, either through MTS labeling or by mutation, inhibited the binding of **1**. These authors proposed that C7.42(386) is near the piperidine ring of **1**. These results are consistent with our dock of **1** in which C7.42(386) is adjacent to the piperidine ring of **1**.<sup>1</sup> The result reported here that **5** can interact with C7.42(386) is also consistent with the localization of C7.42-(386) predicted by Fay and co-workers.<sup>22</sup> The lack of a hydrogen bond with K3.28(192) allows **5** to sit deeper in the binding

crevice. As a result, **5** does not maintain a direct stacking interaction with Y5.39(275), but does maintain aromatic stacking interactions with F3.36(200) and W5.43(279) (Table 1). Although **5** does not stack directly with Y5.39(275), Y5.39(275) has a direct offset parallel stacking interaction with W5.43(279) ( $d = 6.9$  Å). This Y5.39(275)/W5.43(279) stack permits **5** to be part of the larger TMH3-4-5-6 aromatic cluster in the minimized complex.

Figure 7 illustrates the energy minimized complexes, compound **2**/CB1 R (left) and compound **6**/CB1 R (right). The conformation of **2** in this minimized complex is 0.16 kcal/mol above its global minimum (Table 2), whereas the conformation of **6** is 4.57 kcal/mol above its global minimum. Neither

## Scheme 1



**2** nor **6** has a hydrogen-bonding interaction with K3.28(192) in the energy minimized complex (see insets). This is reflected in the small Coulombic energies of interaction listed for **2** and **6** in Table 2. However, both ligands can interact with the TMH3-4-5-6 aromatic cluster. In Figure 7 (left), compound **2** directly stacks with F3.36(200), W5.43(279), and Y5.39(275) (Table 1). This permits the ligand to be part of the TMH3-4-5-6 extended aromatic cluster in the minimized complex.

In Figure 7 (right), the lack of a hydrogen bond with K3.28(192) allows **6** to sit deeper in the binding crevice. As a result, **6** cannot maintain a direct stacking interaction with Y5.39(275). However, **6** does maintain aromatic stacking interactions with F3.36(200), W5.43(279), and W6.48(356) (Table 1). Although **6** does not stack directly with Y5.39(275), Y5.39(275) has a direct offset parallel stacking interaction with W5.43(279)

( $d = 6.7 \text{ \AA}$ ). This Y5.39(275)/W5.43(279) stack permits **6** to be part of the larger TMH3-4-5-6 aromatic cluster in the minimized complex.

**Chemistry.** The conformationally constrained compound **2**, a vinylcyclohexyl analogue of **1**, was synthesized by Wittig olefination as shown in Scheme 1. The route starts with the reported pyrazole ester **1'**,<sup>28</sup> an intermediate in the synthesis of **1**, which was reduced with lithium aluminum hydride to the alcohol **2'**. The latter was converted with  $\text{CBr}_4$  and triphenylphosphine to benzylic bromide **3'** and then to phosphonium salt **4'** with triphenylphosphine. Deprotonation of **4'** with lithium diisopropylamide, to the corresponding stabilized phosphorus ylide, and treatment with cyclohexanecarboxaldehyde afforded the putative olefin **2**. Stabilized ylides, such as those derived from **4'**, typically afford predominantly *trans*-(*E*)-olefins.<sup>29,30</sup>

Proof of the trans geometry was sought via determination of the coupling constant between the vinyl protons in the  $^1\text{H}$  NMR spectrum. However, the chemical shifts of both vinyl protons were very similar, and hence, classic first-order coupling was not observed. Although some evidence of a large coupling constant supportive of a trans olefin was present, a better separation of the resonances was required to prove trans geometry. Examination of various NMR shift reagents revealed that AgFOD resolved the chemical shifts of the two vinyl protons affording a classic first-order spectrum with a coupling constant (16 Hz) indicative of trans geometry. Compound **2** was further characterized by TLC, GC, HPLC, and high-resolution mass spectrometry.

The piperidinoiminomethyl analogue **5** of **1** was synthesized by a condensation reaction shown in Scheme 1. Thus, the above-described alcohol **2'** was oxidized to the aldehyde **6'** by the Swern procedure. Condensation of **6'** with 1-aminopiperidine in the presence of  $\text{MgSO}_4$  afforded **5** as a crystalline, sharp-melting solid. GC and HPLC did not serve to establish homogeneity because of the decomposition under GC conditions and a tailing single peak by HPLC. However, the homogeneity of the product as a single isomer was exhibited by the CMR spectrum, which showed just 18 resonances, consistent with a single component with the structure of the title compound. The structure was further supported by  $^1\text{H}$  NMR, COSY, and HSQC (consistent with the structure), DEPT (6 nonequivalent  $\text{sp}^2$  CH, 3  $\text{CH}_2$ , 1  $\text{CH}_3$ ), and positive ion MS (446 M+, 364 M-84+2, 328 364-HCl, 84 base  $\text{C}_9\text{H}_{10}\text{N}$ ). A ROESY 2D NMR established the E-geometry of the imino double bond by a cross-peak for the through space interaction of the imino hydrogen and the N- $\text{CH}_2$ , only possible for the E-geometry.

The enamine analogue **6** was prepared by a Horner–Wittig type olefination of aldehyde **6'** with the reported (piperidinylmethyl)diphenylphosphine oxide.<sup>31,32</sup> Base promoted addition of the latter with **6'** afforded the diastereomeric phosphinoyl diastereomers **8'** and **9'** as indicated in Scheme 1. Treatment of **9'** with potassium hydride afforded E-enamine **6**, whereas similar treatment of **8'** afforded Z-enamine **10'**. The latter readily isomerized to the thermodynamically more stable E-compound **31** and was not stable at ambient temperature beyond a day. The Z-enamine and its conversion to **6** was observed in the NMR spectrum of the worked up elimination of diphenyl phosphinic acid from **8'**. Compound **6** was characterized by its NMR and ROESY spectra. The latter showed a through space interaction between the enamine  $\beta$ -H and the  $\text{CH}_2$  groups  $\alpha$  to the nitrogen of the piperidine ring, which is only possible with the trans isomer.

When the above elimination of the diphenylphosphinic acid was conducted on each of the pure diphenylphosphinoyl diastereomers, **8'** and **9'**, the corresponding Z- and E-enamines **10'** and **6** were obtained. These were differentiated by an NOE spectroscopy interaction between the enamine  $\beta$ -proton and the piperidinyl methylene protons  $\alpha$  to the nitrogen, which was observed for only one isomer and is possible only for E isomer **6**. Furthermore, Z isomer **10'** was observed to isomerize completely to E isomer **6** overnight in  $\text{CDCl}_3$  solution by NMR. Hence, the mixtures of **8'** and **9'** can be used to prepare pure **6**.

The stability of **5** and **6** to hydrolysis was examined by monitoring for changes in their NMR spectra when stored in aqueous methanol and aqueous THF solvent, respectively (the choice of the water miscible solvents was for optimal resolution of key resonances). Both compounds showed no change during 4 days storage at ambient temperature other than the expected

**Table 3.** Ability of Compound **1** Analogues to Displace [ $^3\text{H}$ ]CP55,940, [ $^3\text{H}$ ]SR141716 and [ $^3\text{H}$ ]WIN55,212-2 from Membranes Prepared from HEK Cell Lines Expressing Human CB1<sup>a</sup>

compd	Displaced against		
	[ $^3\text{H}$ ]CP55,940 $K_i$ (nM)	[ $^3\text{H}$ ]SR141716 $K_i$ (nM)	[ $^3\text{H}$ ]WIN55,212-2 $K_i$ (nM)
<b>1</b>	7.1 (1.8–27)	1.8 (1.3–2.2)	18 (9.2–34)
<b>2</b>	85* (30–243)	31.3 <sup>b</sup>	60* (24–151)
<b>3</b>	5.0 (1.4–18)	1.8 (0.4–7.2)	3.7* (1.3–11)
<b>4</b>	54* (25–116)	30* (8–106)	107* (27–414)
<b>5</b>	57* (19–172)	17* (5.6–57)	19 (7.3–51)
<b>6</b>	258* (24–2725)	213* (38–1218)	223* (55–903)

<sup>a</sup> The inhibition constants were obtained from competition experiments (see Experimental Section). Data are the means and corresponding 95% confidence limits of three or more independent experiments each performed in triplicate. The asterisk (\*) indicates statistically significant differences from the affinity of SR141716 for each radioligand ( $p < 0.05$ ); ND, not determined. The  $B_{\text{max}}$  values were 1.0 (0.8–1.3), 1.7 (1.4–2.0), and 1.2 (0.5–3.0) pmol/mg for CP55,940, SR141716 and WIN55,212-2, respectively. <sup>b</sup> Data from 1.

exchange of the  $\beta$ -enamine proton of **6**. Hence, the compounds are expected to be stable in the aqueous pharmacological studies.

The cyclohexylamide analogue **3** of **1** was reported in the Sanofi patent<sup>33</sup> without details and was prepared for these studies by a detailed route that parallels that used for the synthesis of **1**.<sup>34</sup> Ester **1'** was saponified to acid **11'**, which was converted to acid chloride **12'** (Scheme 1). The latter, without purification since the beginning of the synthesis, was treated with cyclohexylamine to yield **3** after chromatographic purification. Similar to that seen in the synthesis of **1**, the corresponding 1,3-diaryl isomer was also obtained as a minor product and separated during chromatography.<sup>35</sup> The structure of **3** was established by its  $^1\text{H}$  NMR and CMR spectra. Additionally, its shared synthesis scheme with **1** and the proof of structure of the latter serves to establish the structure of **3** by extension. The N-cyclohexyl-N-methylamide analogue (**4**) was similarly prepared and characterized. The  $^1\text{H}$  NMR spectrum of the tertiary amide **4** shows that it exists as a nearly 1:1 mixture of cis and trans amide rotamers in chloroform at ambient temperature (Experimental Section).

**Radioligand Displacement Assays in CB1 WT.** The binding of compounds **1–6** were tested against a hCB1 cell line ( $B_{\text{max}}$  values of 1.0 (0.8–1.3), 1.7 (1.4–2.0), and 1.2 (0.5–3.0) pmol/mg for CP55,940, SR141716, and WIN55,212-2, respectively). The data shown in Table 3 represent  $K_i$  ( $K_d$  value for **1** vs [ $^3\text{H}$ ]SR141716) values of compounds **1–6** displaced against [ $^3\text{H}$ ]CP55,940, [ $^3\text{H}$ ]SR141716, and [ $^3\text{H}$ ]WIN55,212-2 at WT hCB1. Compound **3** retained similar CB1 affinity to **1**, and in the case of competition with [ $^3\text{H}$ ]WIN55,212-2, improved affinity. Compounds **2**, **4**, **5**, and **6** exhibited reduced affinity relative to that of **1**. Compound **6** was found to possess the lowest CB1 affinities in the series against all radioligands. Relative to the affinity of **1**, compound **6** exhibited 36-fold lower affinity versus [ $^3\text{H}$ ]CP55,940, 118-fold lower affinity versus [ $^3\text{H}$ ]SR141716, and 12-fold lower affinity versus [ $^3\text{H}$ ]WIN55,212-2.

The trend in interaction energies shown in Table 2, **3,1** < **5,4** < **2** < **6** is consistent with the trend in  $K_i$  values seen in Table 3 versus [ $^3\text{H}$ ]CP55,940 and is close to the trend in  $K_i$  values versus [ $^3\text{H}$ ]SR141716 (**3,1** < **5** < **4,2** < **6**), but it deviates from the trend in  $K_i$  values versus [ $^3\text{H}$ ]WIN55,212-2 (**3** < **1,5** < **2** < **4** < **6**). It is important to note, however, that pairwise interaction energies may not be directly comparable with changes in affinities. The experimentally measured change in affinity includes not only the strength of ligand–receptor interactions in the newly formed complex but also the possible loss of intrareceptor interactions in the unoccupied receptor

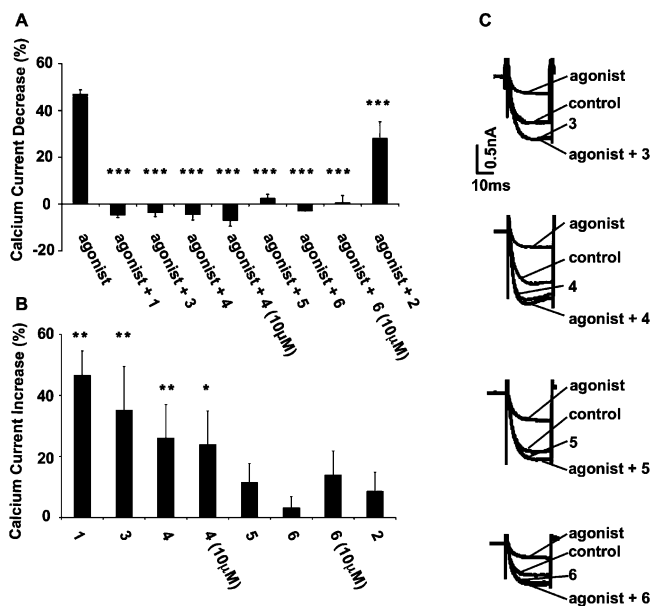


**Figure 8.** Calcium channel assay results for compounds 1–6. (A) Compound 1 and its analogues act as antagonists of CB1 agonist WIN55,212-2. The bar graph shows CB1-mediated  $\text{Ca}^{2+}$  current inhibition as a percentage of control current amplitude in superior cervical ganglion (SCG) neurons injected with rCB1 receptor cDNA. The cannabinoid receptor agonist WIN55,212-2 (1  $\mu\text{M}$ ) inhibits the  $\text{Ca}^{2+}$  current in SCG neurons expressing CB1 cannabinoid receptors. Coapplication of WIN55,212-2 with 1 (1  $\mu\text{M}$ ), 3 (1  $\mu\text{M}$ ), 4 (1 and 10  $\mu\text{M}$ ), 5 (1  $\mu\text{M}$ ), or 6 (1 and 10  $\mu\text{M}$ ) blocked the inhibition of the  $\text{Ca}^{2+}$  current by WIN55,212-2. Compound 2 also blocked the  $\text{Ca}^{2+}$  current inhibition by WIN55,212-2 as previously reported.<sup>1</sup> Therefore, all of the analogues of compound 1 were effective as antagonists of WIN55,212-2. (\*\*\*)  $p \leq 0.0001$  (B) Compounds 1, 3, and 4 act as inverse agonists. The bar graph shows the  $\text{Ca}^{2+}$  current increase as a percentage of control current amplitude in the presence of 1 and its analogues in SCG neurons injected with rCB1 receptor cDNA. The inverse agonist 1 (1  $\mu\text{M}$ ) increased the  $\text{Ca}^{2+}$  current, an effect opposite that of the cannabinoid agonist WIN55,212-2. Compounds 3 (1  $\mu\text{M}$ ) and 4 (1 and 10  $\mu\text{M}$ ) also enhanced the  $\text{Ca}^{2+}$  current indicating that these analogues of 1 act as inverse agonists. Compounds 5 (1  $\mu\text{M}$ ), 6 (1 and 10  $\mu\text{M}$ ), and 2 (1  $\mu\text{M}$ ) did not enhance the  $\text{Ca}^{2+}$  current indicating that these analogues act as neutral antagonists. (paired  $t$ -test \* $p \leq 0.05$ ; \*\* $p \leq 0.01$ ). (C) Superimposed  $\text{Ca}^{2+}$  current traces in the absence (control) and presence of WIN55,212-2 (agonist), the analogue of compound 1 (indicated by compound number), and the analogue of compound 1 plus WIN55,212-2 (analogue number + agonist) for compounds 3, 4, 5, and 6. Current traces for compound 2 can be found in our previous publication (in Figure 7B).<sup>1</sup>

resulting from ligand binding. Although Table 2 should reflect the former, it does not take into consideration the latter.

**Calcium Current Effects of Compounds 1–6 in SCG Neurons.** Figure 8A illustrates that in superior cervical ganglion (SCG) neurons injected with rCB1 cannabinoid receptor cDNA, compound 1 (1  $\mu\text{M}$ ,  $-4.8 \pm 1.3\%$ ,  $n = 8$ ) and its analogues 3 (1  $\mu\text{M}$ ,  $-3.8 \pm 1.3$ ,  $n = 13$ ), 4 (1  $\mu\text{M}$ ,  $-4.5 \pm 2.4\%$ ,  $n = 12$  and 10  $\mu\text{M}$ ,  $-7.0 \pm 2.3\%$ ,  $n = 7$ ), 5 (1  $\mu\text{M}$ ,  $2.6 \pm 1.6\%$ ,  $n = 8$ ), 6 (1  $\mu\text{M}$ ,  $-2.5 \pm 1.0\%$ ,  $n = 15$  and 10  $\mu\text{M}$ ,  $0.7 \pm 3.0\%$ ,  $n = 8$ ), and 2 (1  $\mu\text{M}$ ,  $28.1 \pm 7.0\%$ ,  $n = 6$ ) block the inhibition of the  $\text{Ca}^{2+}$  current elicited by the cannabinoid agonist WIN55,212-2 (1  $\mu\text{M}$ ,  $47.1 \pm 1.7\%$ ,  $n = 76$ ). The data on 2 was previously reported.<sup>1</sup> Thus, compounds 1–6 all acted as antagonists of WIN55,212-2. Compound 1 also acted as an inverse agonist because application of 1 alone significantly increased the  $\text{Ca}^{2+}$  current (1  $\mu\text{M}$ ,  $46.6 \pm 7.9\%$ ,  $n = 8$ ) in SCG neurons expressing CB1 receptors (Figure 8B). Compound 1 acts to reverse the tonic inhibition of  $\text{Ca}^{2+}$  channels resulting from constitutively active CB1 receptors in the absence of

agonists.<sup>13</sup> Compounds 3 (1  $\mu\text{M}$ ,  $35.2 \pm 14.3\%$ ,  $n = 13$ ) and 4 (1  $\mu\text{M}$ ,  $26.1 \pm 10.9\%$ ,  $n = 11$  and 10  $\mu\text{M}$ ,  $23.9 \pm 10.9\%$ ,  $n = 7$ ) also significantly increased the  $\text{Ca}^{2+}$  current in SCG neurons expressing CB1 receptors. Thus, the analogues of compound 1, compounds 3 and 4, also acted as inverse agonists of the CB1 receptor. In contrast, compounds 5 (1  $\mu\text{M}$ ,  $11.5 \pm 6.2\%$ ,  $n = 8$ ), 6 (1  $\mu\text{M}$ ,  $3.2 \pm 3.6\%$ ,  $n = 14$  and 10  $\mu\text{M}$ ,  $13.9 \pm 7.8\%$ ,  $n = 8$ ), and 2 (1  $\mu\text{M}$ ,  $8.6 \pm 6.2\%$ ,  $n = 6$ ) had no significant effect on the amplitude of the  $\text{Ca}^{2+}$  current. Thus, compounds 5, 6, and 2 acted as neutral antagonists because they blocked the effect of the agonist but did not have an effect on their own. Figure 8C shows superimposed  $\text{Ca}^{2+}$  current traces for representative experiments on SCG neurons expressing CB1 receptors in the absence (control) and presence of WIN55,212-2, the analogue of 1, and the analogue of 1 plus WIN55,212-2. These results show that the analogues of 1, compounds 3 and 4, behave as inverse agonists because when given alone they significantly increase the  $\text{Ca}^{2+}$  current, an effect opposite that of the agonist WIN55,212-2, and because they significantly antagonize the effect of WIN55,212-2. In contrast, compounds 5 and 6 behave as neutral antagonists significantly inhibiting the effect of WIN55,212-2, while having no significant effect on their own. Results analogous to those reported here for 5 and 6 were previously obtained for 2 (ref 1, Figure 7B).

## Discussion

**Ligand Binding Affinity.** 5-(4-Chlorophenyl)-3-[(*E*)-2-cyclohexylethenyl]-1-(2,4-dichlorophenyl)-4-methyl-1H-pyrazole (2). In previous work, our modeling studies had suggested that the C-3 substituent of 1 could hydrogen bond with K3.28(192). We designed 2 to be used in a mutant cycle study to test this hypothesis.<sup>1</sup> Compound 2 lacks hydrogen-bonding potential in its C-3 substituent but mimics the geometry of 1 because it has a trans ethylene group replacing the trans amide group in 1 and a cyclohexyl ring replacing the piperidine ring in 1. In the mutant cycle calculation, the C-3 substituent/K3.28(192) interaction is tested by evaluating the effect on affinity when a set of complementary chemical groups is deleted from both ligand (1  $\rightarrow$  2, which removes hydrogen bonding potential from the C-3 substituent) and receptor (WT CB1  $\rightarrow$  K3.28(192)A, which removes the ability of residue 3.28 to offer a hydrogen bond). Scatchard analysis and ligand-binding results for WT CB1 resulted in a  $K_d$  value for 1 at WT CB1 of  $2.3 \pm 1.1$  nM and a  $K_d$  value for 1 in CB1 K3.28(192)A of  $39.6 \pm 10.5$  nM. The  $K_i$  value for 2 binding in cloned human WT CB1 and CB1 K3.28(192)A cell lines versus [ $^3\text{H}$ ]SR141716 was  $31.3 \pm 9.6$  and  $35.2 \pm 1.4$  nM, respectively. The affinity drop for 1 upon the K3.28(192)A mutation and the affinity similarity between 2 at WT CB1 and 1 at K3.28(192)A suggest that there may be a direct interaction between the C-3 substituent of 1 and K3.28(192) (and none between K3.28(192) and 2). However, the key to the determination of whether deletions have occurred between two groups that interact indirectly or directly is the effect produced by simultaneous deletion of both groups (i.e., compound 2/K3.28(192)A). If the modified groups do not interact directly with each other in the WT state, then the effect of the two simultaneous changes will be additive. If the two groups do interact directly in the WT state, there will be no further affinity loss for the compound 2/K3.28(192)A case relative to that of the two cases where one (compound 2/WT CB1) or the other interacting group (compound 1/K3.28(192)A) was deleted. The fact that the  $K_i$  for the double deletion (i.e., compound 2/K3.28(192)A;  $35.2 \pm 1.4$  nM) was not statistically different from either single deletion (compound 1/K3.28(192)A;  $39.6 \pm 10.5$  nM or compound 2/WT CB1;  $31.3 \pm 9.6$  nM) indicated

that there is likely a direct interaction between the C-3 substituent of **1** and K3.28(192) in WT CB1.<sup>1</sup> The present article builds upon these results and seeks to determine which part of the compound **1** C-3 substituent (the carboxamide oxygen or the piperidine nitrogen) has this direct interaction with K3.28(192).

**5-(4-Chlorophenyl)-1-(2,4-dichlorophenyl)-4-methyl-1H-pyrazole-3-(N-cyclohexylcarboxamide) (3).** Compound **3** was designed to test whether the piperidine nitrogen is important for interaction at CB1. In this analogue, the C-3 substituent piperidine ring of **1** is replaced with a cyclohexyl ring. Compound **3**, therefore, retains the C-3 substituent carboxamide oxygen but lacks the piperidine nitrogen. The CB1 affinity data presented in Table 3 indicate that **1** and **3** have comparable affinities versus [<sup>3</sup>H]CP55,940 and [<sup>3</sup>H]SR141716 and that **3** has slightly better CB1 affinity than **1** versus [<sup>3</sup>H]WIN55,212-2. These results are consistent with previous data reported for **3** by the Makriyannis lab.<sup>36</sup> Table 2 indicates that there is no energy expense needed for **3** to dock at CB1. Taken together, these results suggest that the piperidine nitrogen of **1** is not important for the CB1 affinity of **1** but rather that the carboxamide group is key.

**1-[2-(5-(4-Chlorophenyl)-1(2,4-dichlorophenyl)-4-methyl-1H-pyrazole-3-yl)-(E)-vinyl]-piperidine (6).** Compound **6** was designed to test whether the C-3 substituent carboxamide oxygen is important for compound **1** binding at CB1. This analogue differs from **1** in that its carboxamide group has been replaced by a trans ethylene group, which preserves the geometry of the carboxamide group but lacks hydrogen bonding potential. Compound **6**, however, retains a piperidine ring located in the same position as that in **1**. As is clear in Table 3, **6** had the lowest CB1 affinity of all analogues, irrespective of the radioligand used. This result suggests that the carboxamide group (which **6** lacks) is important to the CB1 affinity of **1** and that the piperidine nitrogen is not an important interaction site in the C-3 substituent of **1**. However, we have shown here that the global minimum energy conformer of **6** has its piperidine ring rotated nearly 90° relative to the piperidine ring orientation in the compound **1**/CB1 complex (Figure 4). As shown in Table 2, **6** has an energy expense of 4.57 kcal/mol to adopt the compound **1** piperidine ring orientation in the dock of **1** shown in Figure 5. This by no means is too high of an energy expense to make the dock feasible.<sup>37</sup> Therefore, the significant affinity loss for this analogue likely reflects the double deficit: affinity reduction due to conformational energy expense and affinity reduction due to the lost interaction for the C-3 substituent at CB1.

**5-(4-Chlorophenyl)-1-(2,4-dichlorophenyl)-4-methyl-3-[(E)-piperidinoiminomethyl]-1H-pyrazole (5).** Compound **5** lacks a carboxamide oxygen but has an iminomethyl group replacing the trans amide group of **1** that preserves the trans geometry of this amido group. Compound **5** also retains the piperidine ring. The affinity of **5** for CB1 was reduced relative to **1** by 8-fold when displaced against [<sup>3</sup>H]CP55,940 and 9.4-fold when displaced against [<sup>3</sup>H]SR141716, but not reduced when displaced against [<sup>3</sup>H]WIN55,212-2. Modeling studies suggested that the global minimum energy conformer of **5** had its piperidine ring rotated 90° relative to the piperidine ring orientation in the compound **1**/CB1 complex (Figure 4). As shown in Table 2, **5** has an energy expense of only 1.29 kcal/mol to adopt the compound **1** piperidine ring orientation in the dock of **1** shown in Figure 5. Modeling studies also suggested that the C-3 substituent of **5** is not capable of interacting with K3.28(192) but can form a hydrogen bond with C7.42(386)

(Figure 6). This hydrogen bond may compensate in part for **5**'s inability to form a hydrogen bond with K3.28(192) and moderate the affinity drop seen for **5** when displaced against [<sup>3</sup>H]CP55,940 and [<sup>3</sup>H]SR141716. The compensation provided by the C7.42(386) hydrogen bond appears to have been more significant when [<sup>3</sup>H]WIN55,212-2 was used as the radioligand.

**5-(4-Chlorophenyl)-1-(2,4-dichlorophenyl)-4-methyl-1H-pyrazole-3-(N-cyclohexylcarboxamide) (4).** Compound **4** is an analogue of **3** that differs from **3** only in the replacement of the amide N-H with a N-methyl group. This analogue was synthesized to test if the amide NH may contribute to a binding site interaction with some hydrogen bond acceptor at CB1. As is clear in Table 3, the affinity of **4** is at least 10-fold lower than that of **3** ([<sup>3</sup>H]CP55,940 data). At first inspection, it would seem that one conclusion that could be drawn from this reduction in affinity is that an N-H hydrogen-bonding interaction may be important to the affinity of **1** at CB1. However, the <sup>1</sup>H NMR spectrum of **4** shows that it exists as a nearly 1:1 mixture of cis and trans amide rotamers in chloroform at ambient temperature (see Experimental Section). Our modeling studies indicated that only the trans amide rotamer of **4** is capable of docking at CB1. Furthermore, modeling results for **3** (and for **1**) suggest that the trans amide rotamer of **4** is not capable of adopting a conformation analogous to the docked conformation of **1** (Figure 4) due to steric interference between the pyrazole ring and the N-methyl group (Figure 3). Thus, our modeling studies of **4** (Figures 3 and 6) suggest that its reduction in affinity at CB1 is due to the fact that only the trans amide rotamer can bind at CB1, and this rotamer binds with reduced interaction energy (Table 2).

Taken together, the ligand-binding affinity data and receptor-modeling studies presented here suggest that the piperidine nitrogen of the compound **1** C-3 substituent is not important for interaction at CB1 but that the carboxamide oxygen may be important for interaction at CB1. Furthermore, because our previous mutant cycle study suggested that K3.28(192) has a direct interaction with the C-3 substituent of **1**,<sup>1</sup> we conclude here that the direct interaction between K3.28(192) and **1** is most likely mediated by its carboxamide oxygen.

**Ligand Efficacy.** Calcium channel assay results here suggest that compounds **1–6** can be divided into two categories: inverse agonists (**1**, **3**, and **4**) and neutral antagonists (**2**, **5**, and **6**). This distinction between inverse agonists and neutral antagonists is not correlated with receptor affinity because neutral antagonist **5** has comparable, if not better, CB1 affinity than inverse agonist **4**. For many years, drugs acting at GPCRs were thought to be divided into two classes, agonists and antagonists. It is now apparent that for most GPCRs, the compounds acting at these receptors can exhibit a spectrum of efficacy from inverse agonism through neutral antagonism to agonism.<sup>38</sup> It has been widely assumed for GPCRs that inverse agonists suppress the agonist-independent activity of these receptors by stabilizing the receptor in an inactive state. This depends on receptor activation (receptor-G-protein coupling) occurring in the absence of the agonist, and the inverse agonist suppressing this activity in some way.<sup>38</sup> We have shown previously that the inverse agonism of **1** can be explained by a two state model in which **1** has aromatic stacking interactions in the TMH3-4-5-6 aromatic microdomain in both the inactive and active states of CB1 but can interact with K3.28(192) only in the CB1 inactive state.<sup>1</sup> We report here that the inverse agonists, **3** and **4**, also interact in the TMH3-4-5-6 aromatic microdomain in both the inactive and active (data not shown) states of CB1 but can interact with K3.28(192) only in the CB1 inactive state. Thus, our modeling

studies predict that compounds **1**, **3**, and **4** should have higher affinity for the inactive state of the receptor and behave as inverse agonists. The neutral antagonists, **2**, **5**, and **6**, also can have aromatic stacking interactions in the TMH3-4-5-6 aromatic microdomain in both the inactive and active (data not shown) states of CB1, but these ligands lack the ability to interact with K3.28(192). Thus, our modeling results suggest that such biarylpyrazoles (i.e., compounds **2**, **5**, and **6**) should have a nearly equal preference for R and R\* and, consequently, should fall near the middle of the spectrum of efficacy (inverse agonism → neutral antagonism → agonism).

Why would interaction specifically with K3.28(192) be the key for the production of inverse agonism for this class of compounds at CB1? First, K3.28(192) is a residue capable of acting as a strong hydrogen bond donor, the only such positively charged inward facing residue in the extracellular half of the CB1 TMH bundle. Table 2 illustrates that for compounds **1**, **3**, and **4** (those compounds capable of interacting with K3.28(192)), a major contribution to the overall pairwise interaction energy of each at CB1 is the Coulombic interaction with K3.28(192) (−72.02, −54.64 and −65.99 kJ/mol, respectively). Second, K3.28(192) is attached to a helix that undergoes movement during activation. This means that the location of K3.28(192) should change during the R to R\* transition. It has been shown for rhodopsin and the beta-2-adrenergic receptor that GPCR activation is accompanied by rotations of TMH3 and 6.<sup>25,26,39</sup> Both rotations have been reported to be counterclockwise rotations from the extracellular view. In our activated state model of CB1, K3.28(192) is repositioned to be available in the TMH2-6-7 region, away from the TMH3-4-5-6 aromatic microdomain (Figure 2). So K3.28(192) is available to ligands binding in the TMH3-4-5-6 aromatic microdomain only in the inactive state model. Consistent with this model, mutation studies have indicated that both the CB1 inverse agonist, **1**, and the CB1 agonist WIN55212-2 bind in the TMH3-4-5-6 aromatic microdomain of CB1,<sup>19,27,40</sup> but only **1** interacts with K3.28(192).<sup>1,41</sup> Therefore, results presented here suggest that biarylpyrazoles (such as **1**) capable of a strong interaction with K3.28(192) will favor the inactive state and, thus, behave as inverse agonists.

Finally, the conclusion drawn here that hydrogen bonding of the C-3 substituent carboxamide is important for the production of inverse agonism in this class of compounds is supported by results reported by Jagerovic and coauthors<sup>7</sup> for the triazole, 5-(4-chlorophenyl)-1-(2,4-dichlorophenyl)-3-hexyl-1*H*-1,2,4-triazole. In this analogue, the C-3 substituent (i.e., conventional N-substituted carboxamide) of **1** is replaced with an *n*-hexyl group. Consistent with work reported here, this compound was found to behave as a neutral antagonist in several pharmacological models.

## Experimental Section

**Molecular Modeling.** A recent crystal structure of **1** confirms that the carboxamide of the C3 substituent is in a *trans* geometry (George, C. Laboratory for the Structure of Matter, Naval Research Laboratory. Personal communication). Complete conformational analyses of **1–6** were performed using the semiempirical method, AM1 within the Spartan molecular modeling program (Wavefunction, Inc., Irvine, CA). AM1 6-fold conformer searches were performed for the rotatable bonds in **1** (Chart 1; C-3 substituent: C3-C1' and N2'-N3'; C-5 substituent: C5-C1''; N-1 substituent: N1-C1'''). The corresponding bonds in compounds **2–6** were similarly treated. In a 6-fold AM1 conformer search, local energy minima are identified by rotation of a subject torsion angle through 360° in 60° increments, followed by AM1 energy minimization of each rotamer generated. The use of 6-fold rotations in our protocol was determined by first running lower and higher fold rotations

(2-fold to 16-fold) and comparing the set of minimum energy conformers that resulted from each search. We found that rotations lower than 6-fold missed some conformers seen in higher fold rotations, but 6-fold rotations and higher yielded the same set of conformers. Consequently, all conformer searches reported here for this structurally related set of compounds used 6-fold searches.

An ab initio geometry optimization at the HF 6-31G\* level was then performed for each global minimum energy conformer of **1–6** identified by the AM1 conformational search and for certain other minimum energy conformers identified. The energy separations between conformers reported in the text were calculated using results from these ab initio Hartree–Fock calculations at the 6-31G\* level as encoded in Jaguar (version 6.0, Schrödinger, LLC, New York, NY). To calculate the energy difference between the global minimum energy conformer of each compound and its final docked conformation (the latter as listed in Table 2), rotatable bonds in the global minimum energy conformation were driven to their corresponding value in the final docked conformation and the single point energy of the resultant structure was calculated at the HF 6-31G\* level.

**Receptor Model Construction. Amino Acid Numbering System.** Receptor residues are numbered here using the amino acid numbering scheme proposed by Ballesteros and Weinstein.<sup>42</sup> In this numbering system, the most highly conserved residue in each transmembrane helix (TMH) is assigned a locant of 0.50. This number is preceded by the TMH number and followed in parentheses by the sequence number. All other residues in a TMH are numbered relative to this residue. In this numbering system, for example, the most highly conserved residue in TMH2 of the CB1 receptor is D2.50(163). The residue that immediately precedes it is A2.49(162).

**Model of Inactive (R) Form of CB1.** A model of the inactive (R) form of CB1 was created using the 2.8 Å crystal structure of bovine rhodopsin (Rho).<sup>43</sup> First, the sequence of the human CB1 receptor<sup>44</sup> was aligned with the sequence of bovine rhodopsin (Rho) using the same highly conserved residues as alignment guides, which were used initially to generate our first model of CB1.<sup>45</sup> TMH5 in CB1 lacks the highly conserved proline in TMH5 of Rho. The sequence of CB1 in the TMH5 region was aligned with that of Rho as described previously using its hydrophobicity profile.<sup>45</sup> Helix ends for CB1 were chosen in analogy with those of Rho<sup>43</sup>; TMH1: N1.28(112) – R1.61(145); TMH2: R2.37(150) – H2.68(181); TMH3: S3.21(185) – R3.56(220); TMH4: T4.38(229) – C4.66(257); TMH5: H5.34(270) – K5.64(300); TMH6: R6.28(336) – K6.62(370); TMH7: K7.32(376) – S7.57(401); intracellular extension of TMH7 (Helix 8): D7.59(403) – C7.71(415). With the exception of TMH1, these helix ends were found to be within one turn of the helix ends originally calculated by us and reported in 1995.<sup>45</sup> Changes to the general Rho structure that were necessitated by sequence divergences included the absence of helix kinking proline residues in TMH1 and TMH5 and the lack of a GG motif in TMH2 as well as the presence of extra flexibility in TMH6.

Because TMH6 figures prominently in the R to R\* transition (i.e., activation), we have studied the conformations accessible to TMH6 in CB1 using the Monte Carlo/simulated annealing technique, Conformational Memories (CM).<sup>24</sup> These studies revealed that TMH6 in CB1 has high flexibility because of the small size of residue 6.49 (a Gly) immediately preceding Pro 6.50. Two families of conformers were identified by CM for TMH6 in CB1. Cluster 1 showed a pronounced proline kink (40 members out of 100, 71.2° average kink angle). Cluster 2 contained helices with less pronounced kinks (51 members out of 100; 30.1° average kink angle). A conformer from the more kinked CM family of CB1 TMH6 (Cluster 1) was used in our model of the inactive (R) state of CB1. This conformer was selected (Pro kink angle = 53.1°) so that R3.50(214) and D6.30(338) could form a salt bridge at the intracellular ends of TMHs 3 and 6 in the CB1 TMH bundle. An analogous salt bridge has been shown to be an important stabilizer of the inactive state of the β<sub>2</sub> adrenergic and the 5HT-2a receptors<sup>20,21</sup> and to be present in Rho.<sup>43</sup>

**Model of Active (R\*) Form of CB1.** An R\* CB1 model was created by modification of our Rhodopsin-based model of the inactive (R) form of CB1. This R\* model construction was guided by the biophysical literature on the R to R\* transition in rhodopsin (Rho), the  $\beta$ -2-adrenergic and muscarinic M3 receptors. This literature has indicated that for the  $\beta$ -2-adrenergic receptor, a salt bridge between R3.50 and E6.30 at its intracellular end stabilizes this receptor in its inactive state.<sup>20</sup> Biophysical studies of Rho, the  $\beta$ -2-adrenergic receptor, and the muscarinic M3 receptor have indicated that rotation of TMHs 3<sup>39</sup> and 6<sup>46,47</sup> occurs upon activation. Studies of Rho and the  $\beta$ -2-adrenergic receptor, have indicated that a conformational change in TMH6 occurs upon activation.<sup>25,26,48</sup> Jensen and co-workers<sup>25</sup> demonstrated through fluorescence studies in the  $\beta$ -2-adrenergic receptor that P6.50 in the highly conserved CWXP motif of TMH6 can act as a flexible hinge that mediates the transition from R to R\*. In the R state, these investigators proposed that TMH6 is kinked at P6.50 such that its intracellular end is nearly perpendicular to the membrane and close to the intracellular end of TMH3. The transition to the R\* state is accomplished by the straightening of TMH6 such that the intracellular part of TMH6 moves away from the receptor core and upward toward the lipid bilayer.<sup>25</sup> All of these experimental findings were used to create the R\* model of CB1 described here.

Our conformational memories study of CB1 TMH6 revealed two distinct conformational families for TMH6 that differed in the degree of kinking at CWGP.<sup>24</sup> These conformationally distinct TMH6's were used to create the R and R\* states depicted here. In the R\* bundle, a TMH6 conformer from the second major conformational family (less kinked: 21.8° kink angle) identified by CM<sup>24</sup> was substituted for the TMH6 conformer used in the inactive model of CB1. This conformer was chosen so that the salt bridge in the inactive state between R3.50(214) and D6.30(338) would be broken because of the movement of the intracellular end of TMH6 away from that of TMH3 and out into lipid.<sup>20</sup> In addition, the R\* (active) CB1 bundle was created by rotating TMH3 so that residue 3.41 changes environments.<sup>39</sup> This was accomplished by a 20° counterclockwise (extracellular view) rotation of TMH3 from its orientation in the inactive (R) bundle. TMH6 was also rotated (counterclockwise from extracellular view) so that Cys 6.47 became accessible from inside the binding site crevice.<sup>46</sup>

**Preparation of Helices.** Each helix of the model was capped as the acetamide at its *N*-terminus and as the *N*-methyl amide at its *C*-terminus. Ionizable residues in the first turn of either end of the helix were neutralized, as were any lipid facing charged residues. Ionizable residues were considered charged if they appeared anywhere else in the helix.

**Ligand-Receptor Complex.** Each ligand was docked in the aromatic residue rich TMH3-4-5-6 region of the CB1 R or R\* TMH bundle using interactive computer graphics. Automated docking algorithms are quite useful when little is known about the binding site of a ligand. In the present case, such methods were not used because the binding region in CB1 for **1** (TMH3-4-5-6) and the nature of specific ligand functional group/specific amino acid interactions are known from mutation/chimera studies. The combined information limits the ligand to one particular region of CB1 and to one particular orientation in this region. In the absence of such information, the interactive docking used here would certainly have introduced investigator bias into the results. However, given the following experimental evidence, we consider our approach here to be appropriate. Shire and co-workers<sup>23</sup> have shown in CB1/CB2 chimera studies that the TMH4-EC2-TMH5 region of CB1 contains residues critical for the binding of **1**. Subsequent CB1 F3.36(200)A, W5.43(279)A, and W6.48(356)A mutation studies published by our group indicated that the binding of **1** is affected by each of these mutations, suggesting that these residues are part of the binding site for **1**.<sup>19</sup> Our previous mutant cycle study indicated that K3.28(192) is involved in a direct interaction with the C-3 substituent of **1** in wild-type (WT) CB1.<sup>1</sup> This result fixes the orientation of **1** in the CB1 bundle to be that pictured in Figure 5. Docking of **1-6** in this region and with this orientation followed

by energy minimization refined the initial docked position and interactions for each ligand as indicated in Figures 5-7 and Tables 1-2.

The energy of each ligand/CB1 R or R\* TMH bundle complex was minimized using the AMBER\* united atom force field in Macromodel (version 8.6, Schrödinger, LLC, New York, NY). A distance dependent dielectric, 8.0 Å extended nonbonded cutoff (updated every 10 steps), 20.0 Å electrostatic cutoff, and 4.0 Å hydrogen bond cutoff were used. The first stage of the calculation consisted of 2000 steps of Polak-Ribier conjugate gradient (CG) minimization in which a force constant of 225 kJ/mol was used on the helix backbone atoms in order to hold the TMH backbones fixed, while permitting the side chains to relax. The second stage of the calculation consisted of 100 steps of CG in which the force constant on the helix backbone atoms was reduced to 50 kJ/mol in order to allow the helix backbones to adjust. Stages one and two were repeated with the number of CG steps in stage two incremented from 100 to 500 steps until a gradient of 0.04 kJ/(mol Å<sup>2</sup>) was reached.

**Assessment of Aromatic Stacking Interactions.** Burley and Petsko<sup>49</sup> have reported that aromatic-aromatic ( $\pi$ - $\pi$ ) stacking interactions in proteins operate at distances (*d*) of 4.5-7.0 Å between ring centroids. The angle ( $\alpha$ ) between normal vectors of interacting aromatic rings typically is between 30° and 90°, producing a tilted-T or edge-to-face arrangement of interacting rings. Hunter and co-workers<sup>50</sup> have reported that  $\pi$ - $\pi$  parallel stacking interactions ( $\alpha < 30^\circ$ ) between phenylalanine residues in proteins are favorable if the rings are offset from each other. Residues and/or ligand regions were designated here as participating in an aromatic stacking interaction if they had centroid-to-centroid distances between 4.5 and 7.0 Å. These interactions were further classified as tilted-T arrangements if  $30^\circ \leq \alpha \leq 90^\circ$  and as parallel arrangements for  $\alpha < 30^\circ$ . Parallel arrangements were considered favorable only if the interacting rings were offset from each other.<sup>50</sup> All measurements were made using Maestro (version 7.0, Schrödinger, LLC, New York, NY).

**Assessment of Pairwise Interaction Energies.** After defining the atoms of each ligand as one group (Group 1) and the atoms corresponding to a residue that lines the binding site in the final ligand/CB1 R complex (Figures 5-7) as another group (Group 2), Macromodel (version 8.6, Schrödinger, LLC, New York, NY) was used to output the pair interaction energy (Coulombic and van der Waals) for a given pair of atoms. The pairs corresponding to Group 1 (ligand) and Group 2 (residue of interest) were then summed to yield the interaction energy between the ligand and that residue.

**Molecular Biology/Pharmacology. Cell Transfection.** HEK 293 cells were grown as previously described<sup>51</sup> and transfected by Lipofectamine reagent (Life Technologies) with expression plasmids containing wild-type human CB1 receptor. Stably transfected cells were selected in growth medium containing Geneticin (1 mg/mL).

**Immunofluorescence.** Six selected colonies were expended and tested for receptor expression by immunofluorescence as previously described.<sup>19</sup> Briefly, cells were grown on a poly-D-lysine (20  $\mu$ g/mL) coated cover slip and labeled for 1 h at room temperature with a polyclonal antibody (1:100) generated against the *N*-terminus (1-14) of the human CB1 receptor (Cayman Chemicals). Cells were washed with HEPES-buffered saline composed of (mM): 130 NaCl, 25 D-glucose, 10 HEPES, 5.4 KCl, 1.8 CaCl<sub>2</sub>, and 1 MgCl<sub>2</sub> at pH 7.4 and fixed for 10 min with 4% paraformaldehyde. CB1 receptor antibody was detected with Alexa fluor 488-conjugated goat anti-rabbit secondary antibody (1:500 for 40 min; Molecular Probes). Immunofluorescence was visualized with a fluorescence microscope (Nikon). One cell-line with cell surface labeling similar to that of human CB1 receptor expression was selected for binding experiments.

**Radioligand Binding.** The assay has been previously described.<sup>52</sup> Briefly, cells were harvested in phosphate-buffered saline containing 1mM EDTA and centrifuged at 500g for 5 min. The cell pellet was homogenized and centrifuged twice at 1600g (10 min, 4 °C). The combined supernatants were centrifuged at 39 000g (60 min, 4 °C). The pellet (P2 membrane) was resuspended in a buffer

composed of 50 mM Tris-HCl, 1 mM EDTA, and 3 mM MgCl<sub>2</sub> at pH 7.4 to yield a protein concentration of approximately 2 mg/mL. Membrane preparations were aliquoted and stored at -80 °C. Binding was initiated by the addition of 50 µg of membrane protein into pre-silanized glass tubes containing the radioligand in buffer composed of 50 mM Tris-HCl, 1 mM EDTA, 3 mM MgCl<sub>2</sub>, and 5 mg/mL fatty acid-free BSA at pH 7.4. The radioligands employed in this study were [<sup>3</sup>H]CP55,940 (158 Ci/mmol), [<sup>3</sup>H]SR-141716A (25 Ci/mmol), and [<sup>3</sup>H]WIN55,212-2 (41 Ci/mmol). Nonspecific binding was assessed by the addition of 1 µM unlabeled CP55,940, SR141716, or WIN55,212-2 to the tubes. Binding assays were performed in a total volume of 500 µL for 60 min at 30 °C. Free and bound radioligands were separated by rapid filtration through Whatman GF/C filters that had been soaked in polyethylenimine (0.1%). Filters were shaken for 1 h in 6 mL of scintillation fluid (Fisher) and radioactivity was determined by liquid scintillation counting. Saturation experiments were conducted with 6 concentrations of radioligand ranging from 250 pM to 10 nM. Competition assays were conducted with 1 nM [<sup>3</sup>H]CP55,940 or [<sup>3</sup>H]SR141716 or 2.4 nM [<sup>3</sup>H]WIN55,212-2 and 6 concentrations (0.01 nM to 10 µM) of displacing ligands. *B*<sub>max</sub> and *K*<sub>d</sub> values were calculated by unweighted least-squares nonlinear regression of log concentration values versus binding of pmol/mg of protein. These data was fit to a one-site binding model using GraphPad Prism (GraphPad San Diego, CA). Displacement EC<sub>50</sub> values were determined by unweighted least-squares nonlinear regression of log concentration-percent displacement data and then converted to *K*<sub>i</sub> values using the method of Cheng and Prusoff<sup>53</sup> and analyzed with GraphPad Prism (GraphPad Software, Inc., San Diego, CA).

**Calcium Channel Assay in SCG Neurons. Cannabinoid Receptor Expression and Electrophysiology.** *N*-terminally HA-tagged rat CB1 cannabinoid receptor cDNA in pcDNA3 (from Ken Mackie, University of Washington, Seattle, WA) was injected (100 ng/µL) into the nuclei of isolated rat superior cervical ganglion neurons as previously described.<sup>13,54</sup> The pEGFP-N1 plasmid (10 ng/µL) containing the coding sequence of enhanced green fluorescent protein (Clontech, Palo Alto, CA) was used as a co-injection marker. After an overnight incubation, Ca<sup>2+</sup> currents from injected neurons were recorded in the whole-cell voltage-clamp mode at room temperature (24–26 °C) with an Axopatch 200A patch-clamp amplifier (Axon Instruments, Foster City, CA). The cell membrane capacitance and series resistance were electronically compensated to >80%. Whole-cell currents were low-pass filtered at 5 kHz using the Bessel filter of the clamp amplifier.

Voltage-clamp protocols were generated with a Macintosh computer (Apple Computer, Cupertino, CA) equipped with a PCI-16 Host Interface card connected to an ITC-16 Data Acquisition Interface (Instrutech Corp, Port Washington, NY) using Pulse Control 5.0 XOPs (Bookman, R. J., Herrington, J. D., and Newton, K. R., University of Miami, Miami, FL) with Igor Pro software (WaveMetrics, Lake Oswego, OR). Ca<sup>2+</sup> currents were elicited by voltage steps from a holding potential of -80 mV and digitized at 180 µs per point. A double pulse protocol consisting of two 25 ms steps to +5 mV was used to elicit Ca<sup>2+</sup> currents. The second step to +5 mV was preceded by a 50 ms step to +80 mV. Ca<sup>2+</sup> current amplitudes were isochronally measured 10 ms after the voltage step.

Ca<sup>2+</sup> currents were isolated with an external solution that contained (in mM) 140 tetraethylammonium methanesulfonate, 10 HEPES, 15 glucose, 10 CaCl<sub>2</sub>, 0.0001 tetrodotoxin at pH 7.4 (adjusted with methanesulfonic acid). The intracellular solution contained (in mM) 120 *N*-methyl-D-glucamine, 20 tetraethylammonium chloride, 10 HEPES, 11 EGTA, 1 CaCl<sub>2</sub>, 4 MgATP, 0.1 Na<sub>2</sub>GTP, and 14 phosphocreatine at pH 7.2 (adjusted with methanesulfonic acid). Stock solutions (10 mM) of WIN55,212-2 mesylate (Tocris), **1** (NIDA Drug Supply Program), **3**, **4**, **5**, and **6** were prepared in dimethyl sulfoxide and stored at -20 °C. On the day of the experiment, stock solutions were diluted to 1 µM in external solution and briefly sonicated to facilitate dispersion. Neurons under study were superfused with control external solution or drugs diluted in external solution from an array of glass tubes

controlled by a fast switching device (Warner Instrument Corporation, Hamden, CT).

**Chemistry.** [5-(4-Chlorophenyl)-1-(2,4-dichlorophenyl)-4-methyl-1*H*-pyrazol-3-yl]methanol (**2**). The pyrazole ester **1'** (3.19 g, 7.78 mmol) dissolved in 80 mL of anhydrous ether was added dropwise to a stirred suspension of LiAlH<sub>4</sub> (1.18 g, 31.1 mmol) under nitrogen at ambient temperature. After stirring overnight, TLC analysis (SiO<sub>2</sub>, 1:3 acetone/CH<sub>2</sub>Cl<sub>2</sub>, UV, PMA-Ce<sup>4+</sup>) on an aliquot partitioned between water and ether showed the reaction to be complete. The reaction was quenched by the addition of water (1.18 mL), 15% NaOH (1.18 mL), and water (3.54 mL) with mixing. Filtration from the resulting aluminates and evaporation of the ether afforded 2.84 g (99%) of the title alcohol as an orange solid. <sup>1</sup>H NMR (MeOD, 300 MHz) δ: 7.58 (1H, d, *J* = 2.2 Hz, 3-H), 7.54 (1H, d, *J* = 8.5 Hz, 6-H), 7.46 (dd, 1H, *J* = 2.2, 8.5 Hz, 5-H), 7.37 (dt, 2H, *J* = 8.5, 2.1 Hz, 3',5'-H), 7.20 (dt, 2H, 8.5, 2.0 Hz, 2',6'-H), 4.88 (s, 2H, CH<sub>2</sub>), 2.30 (s, 3H, CH<sub>3</sub>).

**3-(Bromomethyl)-5-(4-chlorophenyl)-1-(2,4-dichlorophenyl)-4-methyl-1*H*-pyrazole (**3'**).** Triphenylphosphine (2.35 g, 8.95 mmol) and carbon tetrabromide (2.97 g, 8.95 mmol) in 50 mL of anhydrous ether were stirred at ambient temperature for 15 min. The pyrazole alcohol **2'** (2.74 g, 7.46 mmol) dissolved in 50 mL of ether was added dropwise to the above phosphonium reagent with stirring followed by a further 40 mL of an ether wash of the dropping funnel. After 3.5 h, TLC analysis (SiO<sub>2</sub>, 1:3 EtOAc/hexane, UV, PMA-Ce<sup>4+</sup>) of a direct aliquot showed the reaction to be complete. Filtration through Celite and rotary evaporation of the volatiles in vacuo afforded a residue that was chromatographed on silica gel (350 g) eluting with a step gradient of CH<sub>2</sub>Cl<sub>2</sub>/hexane (10–50%) that yielded 1.12 g (35%) of the title bromide as a yellow/orange solid. <sup>1</sup>H NMR (MeOD, 300 MHz) δ: 7.56 (1H, d, *J* = 2.0 Hz, 3-H), 7.47 (1H, d, *J* = 8.5 Hz, 6-H), 7.42 (dd, 1H, *J* = 2.2, 8.5 Hz, 5-H), 7.35 (dt, 2H, *J* = 8.6, 2.2 Hz, 3',5'-H), 7.18 (dt, 2H, 8.6, 2.2 Hz, 2',6'-H), 4.61 (s, 2H, CH<sub>2</sub>), 2.14 (s, 3H, CH<sub>3</sub>).

**5-(4-Chlorophenyl)-1-(2,4-dichlorophenyl)-4-methyl-1*H*-pyrazol-3-yl-methyl-triphenylphosphonium Bromide (**4'**).** The pyrazole bromide **3'** (1.0 g, 2.33 mmol) and triphenylphosphine (0.84 g, 3.14 mmol) in 50 mL of dry toluene were heated at reflux under dry nitrogen overnight. After cooling to ambient temperature, the precipitate was filtered and dried in vacuo to afford 1.37 g (85%) of the title salt as a white solid. <sup>1</sup>H NMR (MeOD, 300 MHz) δ: 7.87–7.65 (m, 15 H, Ph<sub>3</sub>), 7.49 (d, 2H, *J* = 2.2 Hz, 3-H), 7.36–7.28 (m, 3H, 5-H, 3',5'-H), 7.16 (d, 1H, *J* = 8.5 Hz, 6-H), 7.03 (d, 2H, *J* = 8.4 Hz, 2',6'-H), 4.87 ("d", 2H, overlapped, CH<sub>2</sub>), 1.62 (s, 3H, CH<sub>3</sub>).

**5-(4-Chlorophenyl)-3-[(*E*)-2-cyclohexylethenyl]-1-(2,4-dichlorophenyl)-4-methyl-1*H*-pyrazole (**2**).** The pyrazole phosphonium salt **4'** (1.3 g, 1.88 mmol) dissolved in 100 mL of anhydrous THF under dry nitrogen was cooled to 0 °C and treated with a 2 M heptane/THF/ethylbenzene solution of LDA (0.940 mL, 1.88 mmol) dropwise with stirring. Cyclohexanecarboxaldehyde (0.228 mL, 1.88 mmol) was added dropwise with stirring. After 15 min, the reaction was warmed to ambient temperature and analyzed by TLC, which showed the reaction to be complete (SiO<sub>2</sub>; acetone or 50% CH<sub>2</sub>-Cl<sub>2</sub>/hexane; UV). The reaction was quenched with 30 mL of saturated NH<sub>4</sub>Cl and extracted with CH<sub>2</sub>Cl<sub>2</sub> (3×). The combined organic layers were dried over Na<sub>2</sub>SO<sub>4</sub> and the solvent removed in vacuo. The residue was chromatographed on a Merck size B silica gel column eluting with 40% CH<sub>2</sub>Cl<sub>2</sub>/hexane to yield 431 mg (52%) of the title trans olefin. <sup>1</sup>H NMR (MeOD, 300 MHz) δ: 7.55 (1H, d, *J* = 1.8 Hz, 3-H), 7.45 (1H, d, *J* = 8.4 Hz, 6-H), 7.42 (dd, 1H, *J* = 2.1, 8.7 Hz, 5-H), 7.35 (dt, 2H, *J* = 8.6, 2.2 Hz, 3',5'-H), 7.17 (dt, 2H, 8.6, 2.2 Hz, 2',6'-H), 6.40 (d\*, 1H, *J* = 15 Hz, vinyl 1-H), 6.34 (dd\*, 1H, *J* = 20, 3 Hz, vinyl 2-H), 2.16 (m, 1H, CH), 2.12 (s, 3H, CH<sub>3</sub>), 1.86–1.68 (m, 4H, CH(CH<sub>2</sub>)<sub>2</sub>), 1.40–1.21 (m, 6H, CH<sub>2</sub>-CH<sub>2</sub>-CH<sub>2</sub>). <sup>1</sup>H NMR (CDCl<sub>3</sub>, 60 mol % AgFOD, 300 MHz) δ: 6.52 (dd, *J* = 6.5, 16.2 Hz, vinyl 2-H), 6.40 (d, *J* = 16.2 Hz, vinyl 1-H); HRMS calcd for C<sub>24</sub>H<sub>23</sub>N<sub>2</sub>Cl<sub>3</sub>: 444.0927; observed: 444.0927. Elemental analysis: theory, C: 64.66, H: 5.20, N: 6.28. Found, C: 64.66, H: 5.24, N: 6.24.

AgFOD = (6,6,7,7,8,8,8-heptafluoro-2,2-dimethyl-3,5-octandi-onato)silver; \*second-order major/minor peaks with the minor peak of the minor doublet were too weak to see (6.25  $\delta$ ). See shift reagent data for resolution of the resonances and definitive determination of the coupling constants.

**5-(4-Chlorophenyl)-1-(2,4-dichlorophenyl)-4-methyl-1H-pyrazole-3-carboxaldehyde (6').** Anhydrous  $\text{CH}_2\text{Cl}_2$  (9 mL) and 2.0 M oxalyl chloride in  $\text{CH}_2\text{Cl}_2$  (3.04 mL; 6.08 mmol) were cooled to  $-78^\circ\text{C}$  with magnetic stirring in an oven dried, 100 mL septum sealed RB Flask under dry nitrogen. Neat DMSO (90.86 mL, 12.1 mmol) was added dropwise over 2 min with stirring. After 2 min, pyrazole alcohol 2' (2.03 g, 5.52 mmol) in 7 mL of  $\text{CH}_2\text{Cl}_2$  was added by syringe over a period of 4 min. The reaction was brought to  $-15^\circ\text{C}$  in an ice/salt bath and stirred for 15 min affording a white precipitate in a pink solution. Triethylamine (3.83 mL, 27.5 mmol) was added to the slurry dropwise and the yellow-green slurry allowed to warm to ambient temperature over 1 h. The reaction was treated with water (50 mL) and  $\text{CH}_2\text{Cl}_2$  (30 mL) and partitioned. The aqueous layer was extracted a second time with  $\text{CH}_2\text{Cl}_2$  (50 mL). The combined organic layers were washed with brine and dried over  $\text{Na}_2\text{SO}_4$ . Filtration and evaporation of the solvent from the filtrate in vacuo gave 1.94 g of a yellow, crisp foam. Chromatography on silica gel (50:1) eluting with 15% ether/hexane gave 0.81 g (40%) of the pure aldehyde, which could be crystallized from  $\text{CH}_2\text{Cl}_2$  or ether/hexane; mp. 116.2–117.5  $^\circ\text{C}$ . TLC (SG-60; 30%  $\text{Et}_2\text{O}$ –hexane; UV),  $R_f$  = 0.33. GC: DB-17, 240  $^\circ\text{C}$ , FID, (99.7%).  $^1\text{H}$  NMR (300 MHz,  $\text{CDCl}_3$ )  $\delta$  10.13 (s, 1H, CHO), 7.46–7.45 (m, 1H, 3-H); 7.35–7.28 (m, 4H, 2',6', 5-, 6-H), 7.07 (d, 2H, 8,6 Hz, 3', 5'-H), 2.35 (s, 3H,  $\text{CH}_3$ ).

**5-(4-Chlorophenyl)-1-(2,4-dichlorophenyl)-4-methyl-3-[(E)-piperidinoiminomethyl]-1H-pyrazole (5).** Aldehyde 6' (192 mg, 0.526 mmol) in 4 mL of dry  $\text{CH}_2\text{Cl}_2$  (from basic  $\text{Al}_2\text{O}_3$ ) was treated with anhydrous 1-aminopiperidine (59 mL, 0.546 mmol) while stirring under a dry nitrogen atmosphere at ambient temperature. After stirring overnight, 19 mg of  $\text{MgSO}_4$  was added followed in 3 h with an additional 30 mg of  $\text{MgSO}_4$ . After 10 min, the reaction was filtered and evaporated in vacuo to yield 222 mg of a crisp, white foam that contained product 5 with only 5% of the starting 6' ( $^1\text{H}$  NMR). Recrystallization from minimal  $\text{CH}_2\text{Cl}_2$  followed by the addition of hexanes or from hexanes/ $\text{Et}_2\text{O}$  (7:3) afforded white, spiked crystals (94 mg); mp 177–178  $^\circ\text{C}$ . Column chromatography of the remaining mother liquor on silica gel (50:1) eluting with 15% ether–hexanes, followed by recrystallization afforded another 83 mg of spiked crystals, for a total of 177 mg (0.370 mmol, 70% yield).

$^1\text{H}$  NMR ( $\text{CDCl}_3$ , 300 MHz)  $\delta$  7.76 ppm (s, 1 H,  $\text{CH}=\text{N}$ ), 7.39 (d,  $J$  = 2.0 Hz, 1H, 3-H), 7.28 (d, 3 H, 2',6',6-H), 7.25 (dd, 1H,  $J$  = 8.5, 2.0 Hz, 5-H); 7.08 (d, 2H,  $J$  = 8.5 Hz, 3',5'-H), 3.16 (m, 4H,  $\text{NCH}_2$ ), 2.30 (s, 3H,  $\text{CH}_3$ ), 1.75 (m, 4 H,  $\text{N-CH}_2\text{-CH}_2$ ), 1.55 (m, 2 H,  $\text{N-CH}_2\text{-CH}_2\text{-CH}_2$ ). CMR ( $\text{CDCl}_3$ , 300 MHz)  $\delta$  10.5 (q), 24.5 (t), 25.5 (t), 52.2 (t), 114.5 (s), 128.1 (d), 128.4 (s), 129.1 (d), 130.1 (d) 130.5 (d), 131.1 (d), 131.2 (d), 133.4 (s), 134.8 (s), 135.6 (s), 136.9 (s), 142.5 (s), 149.7 (s). Nonequivalent carbons designated d (CH), q ( $\text{CH}_3$ ), t ( $\text{CH}_2$ ), and s (quaternary) were derived from comparison of CMR and DEPT spectra.

ROESY (benzene  $d_6$ ): a cross-peak for  $\delta$  7.76 and 3.16 identifies a through space interaction indicative of an E-geometry of the imine double bond. MS =  $m/e$  (446 = M+, 364 = M - 84 + 2, 328 = 364-HCl, 84 = base  $\text{C}_5\text{H}_{10}\text{N}$ ). Elemental analysis: theory, C: 59.01, H: 4.73, N: 12.51. Found, C: 59.30, H: 4.82, N: 12.55. Stability: no change in the  $^1\text{H}$  NMR spectra of 5 in MeOD (22 h); MeOD-20%  $\text{D}_2\text{O}$  (+ 22 h, with crystallization); MeOD- $\text{D}_2\text{O}$ - $\text{CDCl}_3$  (+ 4 days, homogeneous solution).

**1-[5-(4-Chlorophenyl)-1-(2,4-dichlorophenyl)-4-methyl-1H-pyrazole-3-yl]-2-diphenylphosphinoyl-2-piperidinyl-ethanol (8' and 9').** (Piperidinylmethyl)diphenylphosphine oxide (614 mg; 2.05 mmol) and a few crystals of 1,10 phenanthroline indicator was dissolved /suspended in 2 mL of dry THF under dry nitrogen. A few drops of *n*-BuLi (1.6 M in hexanes) were added at  $0^\circ\text{C}$  with stirring until an orange color persisted. This was followed by an additional amount of *n*-BuLi (1.25 mL, 2.0 mmol) affording gas

evolution and a darker orange color. After stirring for 15 min, aldehyde 6' (600 mg; 1.64 mmol) in 2 mL of dry THF was added, turning the solution a dark purple color. The reaction was stirred for an additional hour at  $0^\circ\text{C}$  and then 1 h at room-temperature, monitoring the progress by TLC ( $\text{SiO}_2$ , 1:1  $\text{EtOAc}$ /hex;  $\text{PMA/Ce}^{4+}$ ). The reaction was dissolved in  $\text{CH}_2\text{Cl}_2$  (25 mL) and then washed with 15 mL of  $\text{NH}_4\text{Cl}$  (aq) to achieve pH 8. The aqueous layer was back extracted with 20 mL of  $\text{CH}_2\text{Cl}_2$ . The combined organics were washed two times with brine and then dried over  $\text{Na}_2\text{SO}_4$ . The filtered organics were evaporated to yield 1.26 g of brown foam. Chromatography of the crude product on 60 g of  $\text{SiO}_2$  eluting with 1 L of  $\text{EtOAc}$ /Hex (2:3), then 2 L of  $\text{EtOAc}$ /Hex (1:1), and then 1 L of  $\text{EtOAc}$ , collecting a 125 mL forerun, and then, 20 mL fractions afforded fractions 10–24 containing 327 mg (30%) pure Z-enamine precursor and fractions 51–55 containing 273 mg (25%) of pure E-enamine precursor.

**Z-Enamine Precursor (8').**  $^1\text{H}$  NMR ( $\text{CDCl}_3$ , 300 MHz)  $\delta$  7.94–7.88 (m, 2 H), 7.76–7.69 (m, 2 H), 7.48–7.42 (m, 4 H), 7.35 (d,  $J$  = 2 Hz, 1H), 7.30–7.20 (m, 6 H), 6.99–6.96 (d,  $J$  = 8 Hz, 1 H), 6.76 (d,  $J$  = 2 Hz, 1 H), 5.36–5.31 (dd,  $J$  = 9, 5 Hz, 1H), 4.23–4.19 (dd,  $J$  = 9, 4 Hz, 1 H), 2.95–2.88 (m, 4 H), 1.96 (s, 3 H), 1.42–1.25 (m, 5 H).  $^{31}\text{P}$ NMR ( $\text{CDCl}_3$ , 300 MHz)  $\delta$  30.17 ppm.

**E-Enamine Precursor (9').**  $^1\text{H}$  NMR ( $\text{CDCl}_3$ , 300 MHz)  $\delta$  8.17–8.11 ppm (m, 2 H), 7.99–7.92 (m, 2H), 7.56–7.42 (m, 7H), 7.35 (d,  $J$  = 2 Hz, 1H), 7.27–7.22 (m, 5H), 7.04–7.01 (d,  $J$  = 9 Hz, 2 H), 5.98 (bs, 1 H), 5.62–5.56 (t,  $J$  = 9 Hz, 1 H), 4.30–4.22 (dd,  $J$  = 13 Hz, 1H), 2.61–2.58 (m, 2H), 2.33–2.29 (m, 2H), 2.22 (s, 3H), 1.28–1.14 (m, 7H).  $^{31}\text{P}$ NMR ( $\text{CDCl}_3$ , 300 MHz)  $\delta$  34.09 ppm.

**1-[2-(5-(4-Chlorophenyl)-1-(2,4-dichlorophenyl)-4-methyl-1H-pyrazole-3-yl)-(E)-vinyl]-piperidine (6) and -(Z)-vinyl]-piperidine (10').** (A) An oven dried 5 mL Reactivial was charged with 30% w/w KH/mineral oil (85 mg, 0.64 mmol) under a nitrogen atmosphere, and KH was washed with anhydrous THF (dried through basic  $\text{Al}_2\text{O}_3$ ) to remove the oil. To the KH was added the unpurified diphenylphosphinoyl diastereomers 8' and 9' (410 mg; 0.62 mmol) in 2 mL of THF with stirring under dry nitrogen at ambient temperature. After 10 min of gas evolution, the vial was capped under nitrogen, stirred for 1 h, and then heated at  $45^\circ\text{C}$  for 30 min. The THF was evaporated and partitioned between hexane and water affording a difficult emulsion, which was dispelled with saturated brine. An insoluble material separated in the organic phase and was removed by filtration. In retrospect, this was likely some of product 6. The filtrate was dried over  $\text{Na}_2\text{SO}_4$  and evaporated in vacuo to afford a yellow resin, which afforded both an insoluble (68 mg) and a soluble (117 mg) fraction when triturated with hexane, both of which were identified as enamine 6 (67% combined yield) by NMR. Crystallization from  $\text{CDCl}_3/\text{Et}_2\text{O}$  afforded the product with mp 187.6–188.1  $0^\circ\text{C}$ .

(B) An oven dried 5 mL Reactivial was charged with 30% w/w KH/mineral oil (45 mg, 0.34 mmol) under a nitrogen atmosphere, and KH was washed ( $2 \times 1$  mL) with anhydrous THF (dried through basic  $\text{Al}_2\text{O}_3$ ) to remove the oil. To the KH suspended in 1 mL THF was added the Z-enamine precursor diphenylphosphinoyl diastereomers 8' (150 mg; 0.23 mmol) in 2 mL of THF under dry nitrogen with mixing at ambient temperature. After gas evolution subsided, the reaction became viscous to the extent that it trapped gas bubbles. The capped vial was tapped to dislodge the bubbles and restore stirring. The red mixture with a thick precipitate was stirred for 2 h and then filtered through glass wool followed by a Millipore filter. The THF filtrate was rotary evaporated in vacuo to afford 84 mg (83%) of a yellow resin, which was stored at  $-72^\circ\text{C}$  overnight. The product was identified as enamine 10' by a ROESY NMR experiment, which showed a through space interaction between the vinyl hydrogens that is only possible for the Z-enamine. Also, one of the vinyl hydrogens showed a through space interaction with the pyrazole methyl, whereas the other vinyl hydrogen interacted with the methylenes  $\alpha$  to the piperidine nitrogen consistent with the Z-configuration. By 20 h, Z-enamine 10' converted to E-enamine 6 in the  $\text{CDCl}_3$  solution.

The compound is unstable on silica gel affording the homoaldehyde that would result from hydrolysis of the enamine. The compound is stable in 20% water/THF (both deuterated) at ambient temperature for at least four days (NMR). In deuterated water (20% in THF), the enamine  $\beta$ -proton exchanges 40% in 1 h and completely by 20 h with a resulting collapse of the  $\alpha$ -proton doublet to a singlet. The original NMR spectrum can be regenerated (return of  $\beta$ -proton and  $\alpha$ -proton doublets) by washing the product in  $\text{CDCl}_3$  with  $^1\text{H}_2\text{O}$ .

**E-Enamine (6).**  $^1\text{H}$  NMR ( $\text{CDCl}_3$ , 300 MHz)  $\delta$  7.35–7.36 (d,  $J = 2.2$  Hz, 1 H, Ar–H); 7.04–7.05 (d,  $J = 8.3$  Hz, 2 H, Ar–H); 6.99–7.02 (d,  $J = 14.0$  Hz, 1 H, olefin  $\alpha$  to piperidine); 5.19–5.23 (d,  $J = 14.0$  Hz, 1 H, olefin  $\beta$  to piperidine); 3.05–3.07 (d,  $J = 5.4$  Hz, 4 H,  $\text{N}(\text{CH}_2)_2$ ); 2.07 (s, 3 H, pyr-Me); 1.59 (bs, 6 H,  $(\text{CH}_2)_3$ ).  $^{13}\text{C}$ MR ( $\text{CDCl}_3$ , 300 MHz)  $\delta$  151.79, 141.80, 141.23, 137.00, 134.63, 133.99, 133.17, 130.96, 130.60, 130.05, 128.84, 128.60, 127.61, 111.84, 87.53, 49.37, 25.29, 24.36, 9.11. HPLC (RP C-18 Waters Resolve radial compression column  $10 \mu\text{m} \times 8 \text{mm} \times 10 \text{cm}$ ; 70%  $\text{CH}_3\text{CN}/\text{water}$ ; 280 nm detection; 2.0 mL/min flow rate)  $R_t = 5.7$  min, 100%. Elemental analysis: theory, C: 61.83, H: 4.96, N: 9.40. Found, C: 61.87, H: 5.04, N: 9.27.

**Z-Enamine (10').**  $^1\text{H}$  NMR ( $\text{CDCl}_3$ , 300 MHz)  $\delta$  7.37 ppm (s, 1 H, Ar–H); 7.23–7.25 (d,  $J = 10.0$  Hz, 2 H, Ar–H); 7.04–7.05 (d,  $J = 8.3$  Hz, 2 H, Ar–H); 5.99–6.01 (d,  $J = 10.0$  Hz, 1 H, H  $\alpha$  to piperidine ring); 4.77–4.79 (d,  $J = 10.0$  Hz, 1 H, H  $\alpha$  to pyrazole ring); 3.14 (m, 4 H,  $(\text{CH}_2)_2\text{N}$ ); 2.03 (s, 3 H, Me); 1.51 (m, 6 H,  $(\text{CH}_2)_3$ ).

**5-(4-Chlorophenyl)-1-(2,4-dichlorophenyl)-4-methyl-1H-pyrazole-3-(N-cyclohexylcarboxamide) (3).** The reported acid chloride **12'** (240 mg; 0.55 mmol) dissolved in 10 mL of  $\text{CH}_2\text{Cl}_2$  (dried through basic  $\text{Al}_2\text{O}_3$ ) was treated with cyclohexylamine (dried through basic  $\text{Al}_2\text{O}_3$ ) (89  $\mu\text{L}$ ; 0.825 mmol) at ambient temperature, followed by dry triethylamine (230  $\mu\text{L}$ ; 1.65 mmol) with stirring under a dry nitrogen atmosphere. After 1 h, the reaction was observed by TLC ( $\text{SiO}_2$ ; EtOAc/hexane 1:3, UV) to have a visible yellow spot at the  $R_f$  of **12'**, which did not diminish with either the addition of further cyclohexylamine or upon aqueous work up. The spot was attributed to an impurity in the unpurified **12'**. The reaction was worked up by dilution with 40 mL of  $\text{CH}_2\text{Cl}_2$ , washing the organic layer with 50 mL of 5% aqueous HCl, saturated  $\text{NaHCO}_3$ , and brine. Drying the organic layer with  $\text{Na}_2\text{SO}_4$ , filtration, and evaporation in vacuo gave 300 mg of a foam/resin.

Marginal chromatography on silica gel (20:1) eluting with 10% EtOAc–hexanes afforded mixed fractions, by HPLC (RP-C18 Novapak column,  $\text{CH}_3\text{CN}/\text{H}_2\text{O}$  (3:1), UV detection 280 nm), which when recrystallized from ether–hexane afforded 8 mg of the 1,3-isomer of **3**. Dissolving the remaining material in  $\text{CH}_3\text{CN}/\text{H}_2\text{O}$  (4:1) resulted in crystallization that afforded 133 mg of **3**. The noncrystalline fractions and mother liquors were combined and chromatographed on a Merck size A Lobar prepacked C-18 column eluting with  $\text{CH}_3\text{CN}/\text{H}_2\text{O}$  (4:1), yielding clean separation of the isomers: 1 mg of the 1,3-isomer of **3** and 22 mg of crystalline **3**. The total yield of **3** was 155 mg (61%) and 8 mg (3.5%) of the 1,3-isomer of **3**.

**Compound 3.**  $^1\text{H}$  NMR (300 MHz, MeOD)  $\delta$  7.57 (d, 1H,  $J = 2.2$  Hz, 3-H); 7.54 (d, 1H,  $J = 8.5$  Hz, 6-H); 7.45 (dd, 1H,  $J = 8.5$ , 2.2 Hz, 5-H), 7.37 (d, 2H,  $J = 8.5$  Hz, 2',6'-H); 7.19 (d, 2H,  $J = 8.5$  Hz, 3',5'-H); 3.86 (m, 1H, N–CH); 2.30 (s, 3H,  $\text{CH}_3$ ); 1.96–1.64 (m, 5H, c-hex  $\text{H}_5$ ); 1.48–1.21 (m, 5H, c-hex  $\text{H}'_5$ ). CMR ( $\text{CDCl}_3$ , 300 MHz)  $\delta$  9.8, 25.4, 26.0, 33.6, 48.3, 118.2, 127.8, 128.2, 129.2, 130.7, 131.0, 131.2, 133.4, 135.2, 136.3, 136.4, 143.4, 145.7, 162.2. M.p. 124.3–125.7 °C. TLC ( $\text{SiO}_2$ ; 1:1 EtOAc:Hex; PMA/ $\text{Ce}^{4+}$ )  $R_f = 0.79$ . HPLC RP C-18 Waters Radial Nova Pak; 4  $\mu\text{m}$ , 8 mm  $\times$  10 cm; 75%  $\text{CH}_3\text{CN}$ :  $\text{H}_2\text{O}$ ; 280 nm) 100%,  $R_t = 13$  min, at 2 mL/min.

**1,3-Isomer of 3.**  $^1\text{H}$  NMR (300 MHz,  $\text{CDCl}_3$ )  $\delta$  7.61 (d, 2H,  $J = 8.5$  Hz, 2',6'-H); 7.51 (d, 1H,  $J = 2.2$  Hz, 3-H); 7.47 (d, 1H,  $J = 8.5$  Hz, 6-H); 7.42 (d, 2H,  $J = 8.5$  Hz, 5-H); 7.38 (dd, 1H,  $J = 8.5$ , 2.2 Hz, 3',5'-H); 5.55 (d, 1H,  $J = 8.2$  Hz, NH); 3.88 (m, 1H, N–CH); 2.41 (s, 3H,  $\text{CH}_3$ ); 1.92–1.88 (m, 2H, c-hex  $\text{H}_2$ ); 1.70–1.58 (m, 3H, c-hex  $\text{H}_3$ ); 1.43–1.31 (m, 2H, c-hex  $\text{H}_2$ ); 1.24–1.09

(m, 3H, c-hex  $\text{H}_3$ ).  $^{13}\text{C}$ NMR ( $\text{CDCl}_3$ , 300 MHz)  $\delta$  10.8, 25.0, 25.8, 33.3, 48.8, 115.3, 128.4, 129.2, 129.8, 130.3, 130.5, 131.5, 132.8, 134.6, 136.0, 137.4, 138.3, 151.5, 159.3.

**5-(4-Chlorophenyl)-1-(2,4-dichlorophenyl)-4-methyl-1H-pyrazole-3-(N-cyclohexyl, N-methylcarboxamide) (4).** The reported acid chloride **12'** (200 mg; 0.46 mmol) under dry nitrogen was dissolved in 10 mL of  $\text{CH}_2\text{Cl}_2$  (dried through basic  $\text{Al}_2\text{O}_3$ ) in a septum sealed flask, treated with *N*-cyclohexyl, *N*-methylamine (dried through basic  $\text{Al}_2\text{O}_3$ ) (90  $\mu\text{L}$ ; 0.69 mmol) followed by dry triethylamine (190  $\mu\text{L}$ ; 1.88 mmol) at ambient temperature. The solution was stirred under a dry nitrogen atmosphere for 3 h in a septum sealed flask. The reaction was worked up by dilution with 20 mL of  $\text{CH}_2\text{Cl}_2$ , washing the organic layer with 35 mL of 3% aqueous HCl saturated  $\text{NaHCO}_3$ , and brine to pH 1. Each aqueous layer was back extracted with  $\text{CH}_2\text{Cl}_2$ , which was added to the organic phase before the next washing. Drying the organic layer with  $\text{Na}_2\text{SO}_4$ , filtration, and evaporation in vacuo gave 235 mg of a foam/resin. Chromatography on silica gel (6.5 g) eluting with 10% EtOAc–hexanes (150 mL) followed by 25% EtOAc–hexanes (100 mL) collecting 5 mL fractions afforded 140 mg (64% Th) of the title compound in fractions 22–31. Recrystallization from ether–hexanes provided 113 mg of white crystals; mp 161.6–162.8 °C. Elemental analysis: theory, C: 60.45%, H 5.07%, N 8.81%. Found, C: 60.45%, H 5.06%, N: 8.70%.

TLC ( $\text{SiO}_2$ ; 1:4 Acetone/ $\text{CH}_2\text{Cl}_2$   $R_f = 0.7$  and 1:1 EtOAc/hexane  $R_f = 0.5$ ; PMA/ $\text{Ce}^{4+}$ ) >99%. HPLC (RP C-18 Waters Radial Nova Pak; 4  $\mu\text{m}$ , 8 mm  $\times$  10 cm; 80%  $\text{CH}_3\text{CN}/\text{H}_2\text{O}$ ; 280 nm) 100%,  $R_t = 8.5$  min, at 2 mL/min.

$^1\text{H}$  NMR ( $\text{CDCl}_3$ , 500 MHz)  $\delta$  7.45–7.48 (dd, 1 H,  $J = 13.18$ , 1.95 Hz, Ar–H); 7.30–7.32 (m, 2 H, Ar–H); 7.08–7.27 (m, 4 H, Ar–H); 4.58–4.60 (m, CH, rotamer 46%); 4.04–4.08 (m, CH rotamer 54%); 3.08 (s,  $\text{CH}_3$ , rotamer 46%), 3.03 (s,  $\text{CH}_3$  rotamer 54%); 2.19 (s, 3 H,  $\text{CH}_3$ ); 1.79–1.84 (m, 4 H,  $\text{CH}_2$ ); 1.48–1.70 (m, 4 H,  $\text{CH}_2$ ); 1.08–1.24 (m, 2 H,  $\text{CH}_2$ ). CMR ( $\text{CDCl}_3$ , 300 MHz)  $\delta$  9.4, 25.8, 26.07, 26.14, 27.8, 30.1, 31.5, 31.8, 58.3, 116.2, 116.6, 128.0, 128.2, 129.3, 130.6, 131.0, 133.7, 135.1, 136.0, 136.6, 142.0, 148.1, 164.7, 165.4.

**Acknowledgment.** We gratefully acknowledge the research support from National Institutes of Health/National Institute on Drug Abuse Grants DA03934 and DA000489 to P.R.; DA09978 and DA05274 to M.A.; and DA10350 to D.L.

**Supporting Information Available:** Experimental details of compounds **3**–**6**. This material is available free of charge via the Internet at <http://pubs.acs.org>.

## References

- Hurst, D. P.; Lynch, D. L.; Barnett-Norris, J.; Hyatt, S. M.; Seltzman, H. H.; et al. *N*-(piperidin-1-yl)-5-(4-chlorophenyl)-1-(2,4-dichlorophenyl)-4-methyl-1H-pyrazole-3-carboxamide (SR141716A) interaction with LYS 3.28(192) is crucial for its inverse agonism at the cannabinoid CB1 receptor. *Mol. Pharmacol.* **2002**, *62*, 1274–1287.
- Felder, C. C.; Joyce, K. E.; Briley, E. M.; Mansouri, J.; Mackie, K.; et al. Comparison of the pharmacology and signal transduction of the human cannabinoid CB1 and CB2 receptors. *Mol. Pharmacol.* **1995**, *48*, 443–450.
- Mackie, K.; Lai, Y.; Westenbroek, R.; Mitchell, R. Cannabinoids activate an inwardly rectifying potassium conductance and inhibit Q-type calcium currents in AtT20 cells transfected with rat brain cannabinoid receptor. *J. Neurosci.* **1995**, *15*, 6552–6561.
- Pan, X.; Ikeda, S. R.; Lewis, D. L. Rat brain cannabinoid receptor modulates N-type  $\text{Ca}^{2+}$  channels in a neuronal expression system. *Mol. Pharmacol.* **1996**, *49*, 707–714.
- Rinaldi-Carmona, M.; Barth, F.; Heaulme, M.; Shire, D.; Calandra, B.; et al. SR141716A, a potent and selective antagonist of the brain cannabinoid receptor. *FEBS Lett.* **1994**, *350*, 240–244.
- Lange, J. H.; Kruse, C. G. Keynote review: Medicinal chemistry strategies to CB1 cannabinoid receptor antagonists. *Drug Discovery Today* **2005**, *10*, 693–702.
- Jagerovic, N.; Hernandez-Folgado, L.; Alkorta, I.; Goya, P.; Navarro, M.; et al. Discovery of 5-(4-chlorophenyl)-1-(2,4-dichlorophenyl)-3-hexyl-1h-1,2,4-triazole, a novel in vivo cannabinoid antagonist containing a 1,2,4-triazole motif. *J. Med. Chem.* **2004**, *47*, 2939–2942.

- (8) Lange, J. H.; van Stuijvenberg, H. H.; Coolen, H. K.; Adolfs, T. J.; McCreary, A. C.; et al. Bioisosteric replacements of the pyrazole moiety of rimonabant: synthesis, biological properties, and molecular modeling investigations of thiazoles, triazoles, and imidazoles as potent and selective CB1 cannabinoid receptor antagonists. *J. Med. Chem.* **2005**, *48*, 1823–1838.
- (9) Lange, J. H.; Coolen, H. K.; van Stuijvenberg, H. H.; Dijkman, J. A.; Herremans, A. H.; et al. Synthesis, biological properties, and molecular modeling investigations of novel 3,4-diarylpyrazolines as potent and selective CB(1) cannabinoid receptor antagonists. *J. Med. Chem.* **2004**, *47*, 627–643.
- (10) Plummer, C. W.; Finke, P. E.; Mills, S. G.; Wang, J.; Tong, X.; et al. Synthesis and activity of 4,5-diarylimidazoles as human CB1 receptor inverse agonists. *Bioorg. Med. Chem. Lett.* **2005**, *15*, 1441–1446.
- (11) Muccioli, G. G.; Wouters, J.; Charlier, C.; Scriba, G. K.; Pizzi, T.; et al. Synthesis and activity of 1,3,5-triphenylimidazolidine-2,4-diones and 1,3,5-triphenyl-2-thioxoimidazolidin-4-ones: characterization of new CB1 cannabinoid receptor inverse agonists/antagonists. *J. Med. Chem.* **2006**, *49*, 872–882.
- (12) Meurer, L. C.; Finke, P. E.; Mills, S. G.; Walsh, T. F.; Toupence, R. B.; et al. Synthesis and SAR of 5,6-diarylpyridines as human CB1 inverse agonists. *Bioorg. Med. Chem. Lett.* **2005**, *15*, 645–651.
- (13) Pan, X.; Ikeda, S. R.; Lewis, D. L. SR 141716A acts as an inverse agonist to increase neuronal voltage-dependent Ca<sup>2+</sup> currents by reversal of tonic CB1 cannabinoid receptor activity. *Mol. Pharmacol.* **1998**, *54*, 1064–1072.
- (14) Meschler, J. P.; Kraichely, D. M.; Wilken, G. H.; Howlett, A. C. Inverse agonist properties of N-(piperidin-1-yl)-5-(4-chlorophenyl)-1-(2,4-dichlorophenyl)-4-methyl-1H-pyrazole-3-carboxamide HCl (SR141716A) and 1-(2-chlorophenyl)-4-cyano-5-(4-methoxyphenyl)-1H-pyrazole-3-carboxylic acid phenylamide (CP-272871) for the CB(1) cannabinoid receptor. *Biochem. Pharmacol.* **2000**, *60*, 1315–1323.
- (15) Schlicker, E.; Kathmann, M. Modulation of transmitter release via presynaptic cannabinoid receptors. *Trends Pharmacol. Sci.* **2001**, *22*, 565–572.
- (16) Pertwee, R. G. Inverse agonism and neutral antagonism at cannabinoid CB1 receptors. *Life Sci.* **2005**, *76*, 1307–1324.
- (17) Bouaboula, M.; Perrachon, S.; Milligan, L.; Canat, X.; Rinaldi-Carmona, M.; et al. A selective inverse agonist for central cannabinoid receptor inhibits mitogen-activated protein kinase activation stimulated by insulin or insulin-like growth factor I. Evidence for a new model of receptor/ligand interactions. *J. Biol. Chem.* **1997**, *272*, 22330–22339.
- (18) Leff, P. The two-state model of receptor activation. *Trends Pharmacol. Sci.* **1995**, *16*, 89–97.
- (19) McAllister, S. D.; Rizvi, G.; Anavi-Goffer, S.; Hurst, D. P.; Barnett-Norris, J.; et al. An aromatic microdomain at the cannabinoid CB(1) receptor constitutes an agonist/inverse agonist binding region. *J. Med. Chem.* **2003**, *46*, 5139–5152.
- (20) Ballesteros, J. A.; Jensen, A. D.; Liapakis, G.; Rasmussen, S. G.; Shi, L.; et al. Activation of the beta 2-adrenergic receptor involves disruption of an ionic lock between the cytoplasmic ends of transmembrane segments 3 and 6. *J. Biol. Chem.* **2001**, *276*, 29171–29177.
- (21) Visiers, I.; Ebersole, B. J.; Dracheva, S.; Ballesteros, J.; Sealfon, S. C.; et al. Structural motifs as functional microdomains in G-protein-coupled receptors: Energetic considerations in the mechanism of activation of the serotonin 5-HT<sub>2a</sub> receptor by disruption of the ionic lock of the arginine cage. *Int. J. Quantum Chem.* **2002**, *88*, 65–75.
- (22) Fay, J. F.; Dunham, T. D.; Farrens, D. L. Cysteine residues in the human cannabinoid receptor: only C257 and C264 are required for a functional receptor, and steric bulk at C386 impairs antagonist SR141716A binding. *Biochemistry* **2005**, *44*, 8757–8769.
- (23) Shire, D.; Calandra, B.; Bouaboula, M.; Barth, F.; Rinaldi-Carmona, M.; et al. Cannabinoid receptor interactions with the antagonists SR 141716A and SR 144528. *Life Sci.* **1999**, *65*, 627–635.
- (24) Barnett-Norris, J.; Hurst, D. P.; Buehner, K.; Ballesteros, J. A.; Guarnieri, F.; et al. Agonist alkyl tail interaction with cannabinoid CB1 receptor V6.43/16.46 groove induces a Helix 6 active conformation. *Int. J. Quantum Chem.* **2002**, *88*, 76–86.
- (25) Jensen, A. D.; Guarnieri, F.; Rasmussen, S. G.; Asmar, F.; Ballesteros, J. A.; et al. Agonist-induced conformational changes at the cytoplasmic side of transmembrane segment 6 in the beta 2 adrenergic receptor mapped by site-selective fluorescent labeling. *J. Biol. Chem.* **2001**, *276*, 9279–9290.
- (26) Ghanouni, P.; Steenhuis, J. J.; Farrens, D. L.; Kobilka, B. K. Agonist-induced conformational changes in the G-protein-coupling domain of the beta 2 adrenergic receptor. *Proc. Natl. Acad. Sci. U.S.A.* **2001**, *98*, 5997–6002.
- (27) McAllister, S. D.; Tao, Q.; Barnett-Norris, J.; Buehner, K.; Hurst, D. P.; et al. A critical role for a tyrosine residue in the cannabinoid receptors for ligand recognition. *Biochem. Pharmacol.* **2002**, *63*, 2121–2136.
- (28) Barth, F.; Casellas, P.; Congy, C.; Martinez, S.; Rinaldi, M.; et al. Substituted N-Piperidino-3-Pyrazolecarboxamide. Eur. Pat. Appl. 656354, A1, 1995.
- (29) Carey, F. A.; Sundberg, R. J. *Advanced Organic Chemistry Part B: Reactions and Synthesis*; 3rd ed.; Plenum Press: New York and London, 1990; p 98.
- (30) Vedejs, E.; Peterson, M. J. Stereochemistry and Mechanism in the Wittig Reaction. *Topics in Stereochemistry*; John Wiley & Sons: New York, 1994; pp 1–157.
- (31) Broekhof, N. L. J. M.; Jonkers, F. L.; van der Gen, A. Enamine synthesis by the Horner-Wittig Reaction. *Tetrahedron Lett.* **1979**, *20*, 2433–2436.
- (32) Broekhof, N. L. J. M.; Elburg, P. v.; Gen, A. v. d. Recl.: *J. R. Neth. Chem. Soc.* **1984**, *103*, 312–316.
- (33) Barth, F.; Casellas, P.; Congy, C.; Martinez, S.; Rinaldi, M.; et al. Pyrazole derivatives as cannabinoid receptor agonists. *CAPLUS*; Sanofi: US 5624941 A 19970429 CAN 127:5085 AN 1997:311258, 1997.
- (34) Seltzman, H. H.; Carroll, F. I.; Burgess, J. P.; Wyrick, C. D.; Burch, D. F. Synthesis, spectral studies and tritiation of the cannabinoid antagonist SR141716A. *J. Chem. Soc., Chem. Commun.* **1995**, 1549–1550.
- (35) Seltzman, H. H.; Carroll, F. I.; Burgess, J. P.; Wyrick, C. D.; Burch, D. F. Tritiation of SR141716 by metalation-iodination-reduction: tritium-proton NOE study. *J. Labelled Compd. Radiopharm.* **2002**, *45*, 59–70.
- (36) Lan, R.; Liu, Q.; Fan, P.; Lin, S.; Fernando, S. R.; et al. Structure–activity relationships of pyrazole derivatives as cannabinoid receptor antagonists. *J. Med. Chem.* **1999**, *42*, 769–776.
- (37) Perola, E.; Charifson, P. S. Conformational analysis of drug-like molecules bound to proteins: An extensive study of ligand reorganization upon binding. *J. Med. Chem.* **2004**, *47*, 2499–2510.
- (38) Strange, P. G. Mechanisms of inverse agonism at G-protein-coupled receptors. *Trends Pharmacol. Sci.* **2002**, *23*, 89–95.
- (39) Lin, S. W.; Sakmar, T. P. Specific tryptophan UV-absorbance changes are probes of the transition of rhodopsin to its active state. *Biochemistry* **1996**, *35*, 11149–11159.
- (40) Song, Z. H.; Slowey, C. A.; Hurst, D. P.; Reggio, P. H. The difference between the CB(1) and CB(2) cannabinoid receptors at position 5.46 is crucial for the selectivity of WIN55212-2 for CB(2). *Mol. Pharmacol.* **1999**, *56*, 834–840.
- (41) Song, Z. H.; Bonner, T. I. A lysine residue of the cannabinoid receptor is critical for receptor recognition by several agonists but not WIN55212-2. *Mol. Pharmacol.* **1996**, *49*, 891–896.
- (42) Ballesteros, J. A.; Weinstein, H. *Integrated Methods for the Construction of Three-Dimensional Models and Computational Probing of Structure Function Relations in G Protein-Coupled Receptors. Methods in Neuroscience*; Academic Press: San Diego, CA, 1995; pp 366–428; Chapter 319.
- (43) Palczewski, K.; Kumasaka, T.; Hori, T.; Behnke, C. A.; Motoshima, H.; et al. Crystal structure of rhodopsin: A G protein-coupled receptor. *Science* **2000**, *289*, 739–745.
- (44) Gerard, C. M.; Mollereau, C.; Vassart, G.; Parmentier, M. Molecular cloning of a human cannabinoid receptor which is also expressed in testis. *Biochem. J.* **1991**, *279*, 129–134.
- (45) Bramblett, R. D.; Panu, A. M.; Ballesteros, J. A.; Reggio, P. H. Construction of a 3D model of the cannabinoid CB1 receptor: Determination of helix ends and helix orientation. *Life Sci.* **1995**, *56*, 1971–1982.
- (46) Javitch, J. A.; Fu, D.; Liapakis, G.; Chen, J. Constitutive activation of the beta2 adrenergic receptor alters the orientation of its sixth membrane-spanning segment. *J. Biol. Chem.* **1997**, *272*, 18546–18549.
- (47) Ward, S. D.; Hamdan, F. F.; Bloodworth, L. M.; Siddiqui, N. A.; Li, J. H.; et al. Use of an in situ disulfide cross-linking strategy to study the dynamic properties of the cytoplasmic end of transmembrane domain VI of the M(3) muscarinic acetylcholine receptor. *Biochemistry* **2006**, *45*, 676–685.
- (48) Farrens, D. L.; Altenbach, C.; Yang, K.; Hubbell, W. L.; Khorana, H. G. Requirement of rigid-body motion of transmembrane helices for light-activation of rhodopsin. *Science* **1996**, *274*, 768–770.
- (49) Burley, S. K.; Petsko, G. A. Aromatic–aromatic interaction: a mechanism of protein structure stabilization. *Science* **1985**, *229*, 23–28.
- (50) Hunter, C. A.; Singh, J.; Thornton, J. M. Pi-pi interactions: the geometry and energetics of phenylalanine-phenylalanine interactions in proteins. *J. Mol. Biol.* **1991**, *218*, 837–846.

- (51) Tao, Q.; McAllister, S. D.; Andreassi, J.; Nowell, K. W.; Cabral, G. A.; et al. Role of a conserved lysine residue in the peripheral cannabinoid receptor (CB2): evidence for subtype specificity. *Mol. Pharmacol.* **1999**, *55*, 605–613.
- (52) Tao, Q.; Abood, M. E. Mutation of a highly conserved aspartate residue in the second transmembrane domain of the cannabinoid receptors, CB1 and CB2, disrupts G-protein coupling. *J. Pharmacol. Exp. Ther.* **1998**, *285*, 651–658.
- (53) Cheng, Y.; Prusoff, W. H. Relationship between the inhibition constant ( $K_i$ ) and the concentration of inhibitor which causes 50% inhibition ( $IC_{50}$ ) of an enzymatic reaction. *Biochem. Pharmacol.* **1973**, *22*, 3099–3108.
- (54) Vasquez, C.; Lewis, D. L. The CB1 cannabinoid receptor can sequester G-proteins, making them unavailable to couple to other receptors. *J. Neurosci.* **1999**, *19*, 9271–9280.

JM060446B